NASA TECHNICAL NOTE

NASA TN D-8242

NASA TN D-8242

AERODYNAMIC CHARACTERISTICS OF A VANE FLOW ANGULARITY SENSOR SYSTEM CAPABLE OF MEASURING FLIGHTPATH ACCELERATIONS FOR THE MACH NUMBER RANGE FROM 0.40 TO 2.54

Glenn M. Sakamoto

Dryden Flight Research Center
Edwards, Calif. 93523

NATIONAL AERONAUTICS AND SPACE ADMINISTRATION • WASHINGTON, D. C. • MAY 1976

1. Report No	2. Government Accession No.	3. Recipient's Catalog No.
NASA TN D-8242		

4. Title and Subtitle	5. Report Date
AERODYNAMIC CHARACTERISTICS OF A VANE FLOW ANGULARITY SENSOR SYSTEM CAPABLE OF MEASURING FLIGHTPATH ACCELERATIONS FOR THE MACH NUMBER RANGE FROM 0.40 TO 2.54	May 1976
	6. Performing Organization Code

7. Author(s)	8. Performing Organization Report No.
Glenn M. Sakamoto	H-900
	10. Work Unit No.

9. Performing Organization Name and Address	517-51-01
NASA Flight Research Center P.O. Box 273 Edwards, California 93523	11. Contract or Grant No.
	Technical Note
	13. Type of Report and Period Covered

12. Sponsoring Agency Name and Address	
National Aeronautics and Space Administration Washington, D.C. 20546	14. Sponsoring Agency Code

15. Supplementary Notes

16. Abstract

This report presents the results of a wind tunnel investigation of the aerodynamic characteristics of a vane flow angularity sensor system capable of measuring flightpath accelerations. The aerodynamic characteristics of the angle of attack vane and the angle of sideslip vane are summarized. The test conditions ranged in free stream Mach number from 0.40 to 2.54, in angle of attack from -2° to 22°, in angle of sideslip from -2° to 12°, and in Reynolds number from

5.9×10^6 per meter $(1.8 \times 10^6$ per foot) to 18.0×10^6 per meter $(5.5 \times 10^6$ per foot).

The results of the wind tunnel investigation are compared with results obtained with similar vane configurations. Comparisons with a NACA vane configuration are also made. In addition, wind tunnel-derived upwash for the test installation is compared with analytical predictions.

17. Key Words (Suggested by Author(s))	18. Distribution Statement
Wind tunnel tests Vane flow direction sensors Upwash corrections	Unclassified - Unlimited Category: 06

19. Security Classif. (of this report)	20. Security Classif. (of this page)	21. No. of Pages	22. Price*
Unclassified	Unclassified	43	$3.75

*For sale by the National Technical Information Service, Springfield, Virginia 22161

AERODYNAMIC CHARACTERISTICS OF A VANE FLOW ANGULARITY

SENSOR SYSTEM CAPABLE OF MEASURING FLIGHTPATH ACCELERATIONS

FOR THE MACH NUMBER RANGE FROM 0.40 TO 2.54

Glenn M. Sakamoto
Flight Research Center

SUMMARY

A wind tunnel investigation was conducted on a vane flow angularity sensor system capable of measuring flightpath accelerations in an attempt to define the aerodynamic characteristics of the vanes. The measurements of the angle of attack and angle of sideslip vanes both showed error throughout the Mach number range tested. The vane errors were greatly affected by Mach number. The errors due to Mach number were largest at transonic Mach numbers for the angle of attack vanes. The errors were largest at high supersonic Mach numbers for the angle of sideslip vane and resulted from shock interference.

The characteristics of the effects of Mach number on both vanes indicated that the vane assemblies were in such close proximity to each other that there was considerable mutual interference. A comparison of the calibration obtained for this test installation with a calibration obtained for a similar system substantiates this finding.

A comparison of the calibrations for the tested vanes and standard NACA vanes showed their aerodynamic characteristics to be similar. This similarity was observed despite significant differences in the vane configurations. The frequency and damping of the tested vanes were one-half those of the NACA vanes.

A comparison of wind tunnel-derived nose boom upwash with analytical predictions showed that the prediction method provided reasonable estimates of upwash over the Mach number range tested. The prediction method did not account for the shock-to-vane interactions manifest in the wind tunnel data.

The results of this calibration verify and extend previously obtained wind tunnel results for a similar configuration.

INTRODUCTION

Aircraft flight test programs require the precise measurement of angle of attack and angle of sideslip, since these measurements yield information concerning the aircraft's flight status and are also essential to many of the subsequent analyses. One of the most common measurement systems is a nose boom-mounted vane system with a configuration similar to the NACA design described in references 1 to 3. Recently, flow direction vanes have also been used as the mount for linear accelerometers, which are used to sense vehicle flightpath acceleration. Flow angularity vanes equipped with flightpath accelerometers were developed during a wind tunnel program conducted at the Arnold Engineering Development Center (AEDC) in Tullahoma, Tenn. (refs. 4 to 6) and are significantly different in design from conventional NACA vanes.

The new sensor system was used in a joint NASA/Air Force transonic aircraft technology (TACT) program at Edwards, Calif. This was NASA's first experience with a vane flow angularity sensor system capable of measuring flightpath accelerations. Since unusual variations in angle of attack and angle of sideslip were observed in limited wind tunnel tests of a similar system (refs. 4 to 6), in 1973 the entire nose boom assembly for the TACT airplane was calibrated in the Unitary Plan Wind Tunnel facility at the NASA Ames Research Center.

This report presents the results of the angle of attack and angle of sideslip vane calibration obtained at Ames. During the investigation, Mach number ranged from 0.40 to 2.54, angle of attack varied from $-2°$ to $22°$, and angle of sideslip varied from $-2°$ to $12°$. The calibration data from these tests are compared with previous calibrations obtained at AEDC. The calibration data are also compared with a calibration for a NACA vane configuration to identify areas of aerodynamic similarity. Finally, a comparison is made between the nose boom upwash predicted by wind tunnel results and those predicted by an analytical prediction technique.

SYMBOLS

Physical quantities in this report are given in the International System of Units (SI) and parenthetically in U.S. Customary Units. The measurements were taken in Customary Units. Factors relating the two systems are presented in reference 7.

E_α angle of attack vane error, $\alpha_i - \alpha_t$, deg

E_β angle of sideslip vane error, $\beta_i \cos \alpha_t - \beta_t$, deg

f_n natural frequency, Hz

h altitude, m (ft)

M Mach number

R	radial distance from the nose boom centerline to the vane center of pressure (fig. 16), approximately 20 cm (7.87 in.)
R'	approximate radial distance from the nose boom centerline to the shock wave along the vane hinge line (fig. 16), cm (in.)
R_0	approximate radial distance from the nose boom centerline to the shock wave just inboard of the vane (fig. 16), cm (in.)
Re/l	unit Reynolds number, per m (per ft)
u, v, w	components of velocity, V (fig. 24), m/sec (ft/sec)
V	velocity, m/sec (ft/sec)
x, y, z	rectangular coordinates of the body axes (fig. 24)
α	angle of attack, deg
β	angle of sideslip, deg
ζ	damping ratio
$\Delta\alpha_{vf}$	angle of attack vane float, deg
$\Delta\alpha/\alpha$	nose boom upwash, $\dfrac{\alpha_i - \alpha_t}{\alpha_i}$
$\Delta\beta_{vf}$	angle of sideslip vane float, deg
$\Delta\beta/\beta$	nose boom sidewash, $\dfrac{\beta_i^* - \beta_t}{\beta_i^*}$

Subscripts:

e	equivalent
i	indicated
t	true
∞	free stream

Superscript:

$*$	transformed from nose boom axis to wind axis

The subject of this investigation is a flow angularity sensor system consisting of a pitot-static probe system for measuring static and total pressures, vane assemblies for measuring angle of attack and angle of sideslip, and a dual-axis accelerometer capable of measuring longitudinal and normal acceleration along a flightpath. The flow angularity sensor is shown in figure 1 and its dimensions are given in figure 2.

Figure 1. Photograph of flow angularity sensor system.
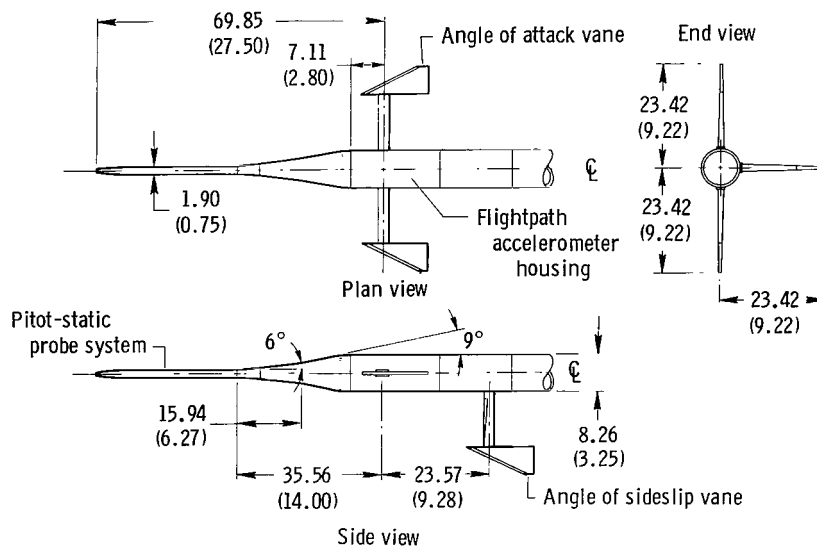
Figure 2. Dimensional details of flow angularity sensor in three views. Dimensions are in centimeters (inches).

4

The flow angularity vanes are flat plates with swept, beveled leading edges. The vanes are fixed to rotating, aerodynamically contoured posts. The dimensions of the vanes, which were identical for angle of attack and angle of sideslip, are shown in figure 3. Further details concerning the design and selection of this vane configuration are given in reference 4.
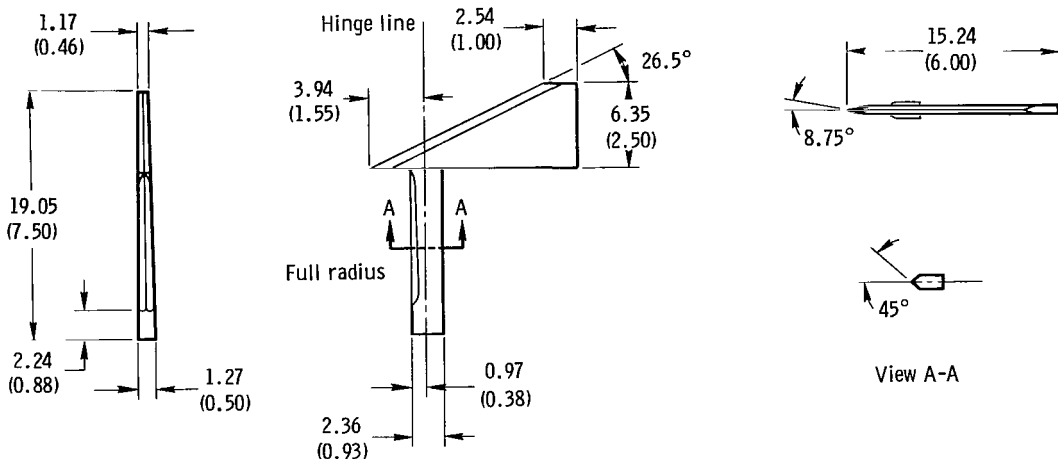
Figure 3. Dimensional details of vanes in three views.
Dimensions are in centimeters (inches).

The angle of attack vanes are symmetrically arranged. Angle of attack measurements were taken with respect to the left vane as seen in normal plan view orientation. The angle of sideslip vane assembly is 23.57 centimeters (9.28 inches) to the rear of the angle of attack vane assembly. Because of the size of the flightpath accelerometer assembly, the angle of attack vanes for this particular system are physically constrained to deflections of -5° and 28° relative to the centerline of the housing. Figure 4 illustrates the arrangement of the flightpath accelerometer assembly.
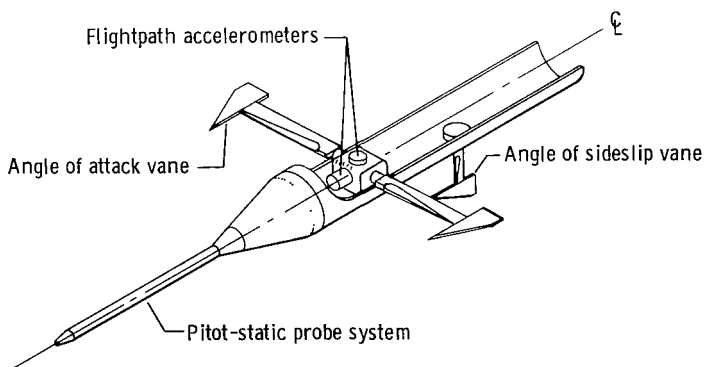
Figure 4. Schematic of flightpath accelerometer assembly.

WIND TUNNEL TESTS

Tunnel Description

The flow angularity calibration was conducted in the 11-Foot Transonic and the 9- by 7-Foot Supersonic Wind Tunnels in the NASA Ames Unitary Plan Wind Tunnel facility. Both are closed circuit, continuous flow, variable density tunnels. The transonic leg has a Mach number capability from 0.40 to 1.40, and the supersonic leg has a Mach number range from 1.55 to 2.55. Both tunnels are described in detail in reference 8.

Static Tunnel Calibration

The strut-mounted nose boom assembly (fig. 5) together with the externally controlled drive unit were first calibrated under static conditions. The nose boom assembly was put in a level position and statically loaded in the angle of attack plane to determine nose boom and wind tunnel balance flexibility in the presence of aerodynamic lift. An upward aerodynamic load of approximately 445 newtons (100 pounds), which was determined from an equation in reference 9, was applied. The effect of this load was determined to be negligible. No side loads were applied in the angle of sideslip plane.
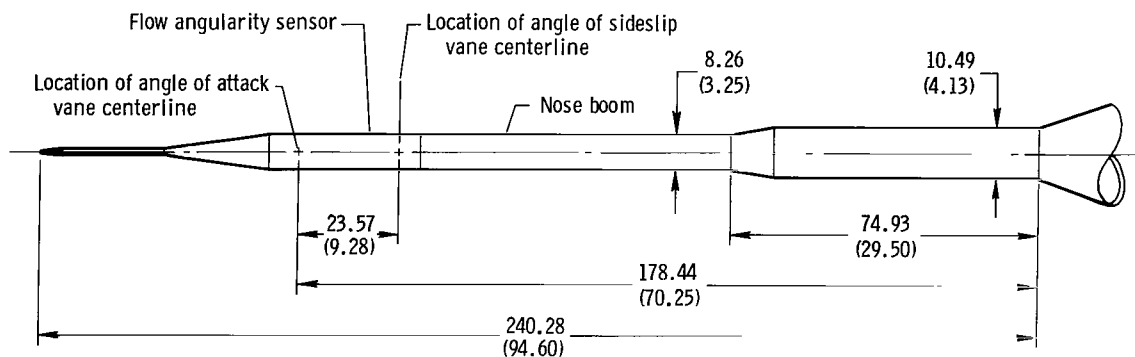
*Figure 5. Schematic of wind tunnel nose boom installation.
Dimensions are in centimeters (inches).*

The externally controlled drive unit was calibrated by hard mounting a laser unit to the nose boom and using it to trace a locus of the strut position on a fixed target located upstream of the test section. In addition, a split-bubble clinometer accurate to 6 seconds was mounted on the boom and simultaneous readings were taken from it and the vane synchro transmitter. A bubble level accurate to 3 seconds was affixed to the angle of attack vane to indicate the level vane condition. Hysteresis was detected in the control drive unit and was minimized by always approaching the angle of attack set in the tunnel from a higher angle of attack.

Test Procedure

The center of rotation in the angle of attack plane was at the angle of attack vane centerline such that at zero angle of sideslip the orientation of the nose boom assembly was identical to the tunnel centerline. In the angle of sideslip plane, the center of rotation was in the strut body such that all nonzero angles of sideslip were off the tunnel centerline.

Upright and inverted tests were performed to establish tunnel flow angularity corrections. The angle of attack set in the tunnel was always approached from a higher angle of attack to minimize mechanical and aerodynamic hysteresis.

Schlieren photographs were taken at certain Mach number, angle of attack, and angle of sideslip conditions in both tunnels for shock wave visualization. Emphasis was placed on the transonic Mach number region to define compressibility effects on the vanes and on Mach numbers near 2.0, where sideslip vane error reversal was known to occur (refs. 4 to 6).

Test Conditions

The wind tunnel test conditions are summarized in table 1. Mach number ranged from a nominal 0.40 to 2.54. Angle of attack ranged from -2° to 22° in the 11-Foot Tunnel and from -2° to 16° in the 9- by 7-Foot Tunnel. Angle of sideslip ranged from -2° to 12° in both tunnels. The angles of attack and angles of sideslip set in the tunnel were varied in 2° increments. Reynolds number ranged from 5.9×10^6 per meter (1.8×10^6 per foot) to 18.0×10^6 per meter (5.5×10^6 per foot). Several Reynolds numbers were tested at free stream Mach numbers of 0.90, 1.30, and 1.51 to assess the effects of unit Reynolds number.

Instrumentation, Data Reduction, and Accuracy

The instrumentation already installed in the nose boom assembly was adequate for the flow angularity calibration. Flow angularity measurements were obtained from synchro transmitters in the angle of attack and angle of sideslip vanes. Simultaneous free stream total and static pressure measurements were obtained from the pitot-static probe system. The measurements were recorded on standard wind tunnel recorders.

The flow angularity calibration data for the angle of attack and angle of sideslip vanes were corrected for the effects of wind tunnel flow angularity. Corrections for boom bending based on the analytical method described in reference 10 were applied to the angle of attack and angle of sideslip data but in general were negligible. In addition, the angle of sideslip data, which were based on the nose boom axis, were transformed to the wind axis by using the following equation:

$$\beta_i{}^* = \beta_i \cos \alpha_t$$

This equation is derived in appendix A.

TABLE 1. – WIND TUNNEL TEST VARIABLES

Wind tunnel	M_∞	Re/l, per m (per ft)		α_t, deg	β_t, deg
11-Foot	0.40	6.6×10^6	(2.0×10^6)	-2 to 22	-2 to 12
	0.60	8.5	(2.6)		
	0.80	6.9	(2.1)		
	0.90	6.6	(2.0)		
	0.90	10.8	(3.3)		
	0.90	18.0	(5.5)		
	0.95	5.9	(1.8)		
	1.05	9.2	(2.8)		
	1.10	9.5	(2.9)		
	1.20	10.2	(3.1)		
	1.30	7.9	(2.4)		
	1.30	12.1	(3.7)		
9- by 7-Foot	1.51	6.6	(2.0)	-2 to 16	-2 to 12
	1.51	13.1	(4.0)		
	1.71	12.1	(3.7)		
	1.91	14.1	(4.3)		
	2.11	13.8	(4.2)		
	2.31	13.4	(4.1)		
	2.54	11.8	(3.6)		

Estimates of the accuracies of the wind tunnel or reference variables (M_∞, α_t, and β_t) and the vane measurements (α_i and β_i) are presented in table 2. Table 2 also presents estimates of the accuracies of the angle of attack and angle of sideslip vane errors (E_α and E_β) obtained by performing a root-sum-square error analysis on the accuracies of the reference and measured variables.

RESULTS AND DISCUSSION

Wind Tunnel Test Results

The following discussion concerns the calibration data obtained for the angle of attack and angle of sideslip vanes. The complete calibration is summarized in appendix B. An analysis of the flow field about the test vanes was performed to correlate the variations observed in the calibration data with the variations in the

TABLE 2. - ESTIMATED ACCURACIES OF THE
WIND TUNNEL TEST VARIABLES

Wind tunnel	Accuracy of -						
	Wind tunnel variables			Vane measurement		Vane error	
	M_∞	α_t, deg	β_t, deg	α_i, deg	β_i, deg	E_α, deg	E_β, deg
11-Foot	±0.005	±0.01	±0.15	±0.05	±0.05	±0.05	±0.16
9- by 7-Foot	±0.10	±0.05	±0.05	±0.05	±0.05	±0.07	±0.07

local flow observed in Schlieren photographs. Since the quality of the Schlieren photographs was generally poor, sketches of the photographs are presented instead of the photographs themselves.

Angle of attack calibration data. – The calibration data obtained for the angle of attack vane at a zero angle of sideslip ($\beta_t = 0°$) are summarized in figure 6 as a function of indicated angle of attack, α_i, for each Mach number tested. The calibration depicts the aerodynamic characteristics of the angle of attack vanes in terms of the vane error, E_α. The data appear to indicate vane float, nose boom upwash, and Mach number effects. As the angle of attack of the nose boom assembly increased, the angle of attack measurements appeared to become influenced by the aerodynamic upwash field of the nose boom installation. The vane aerodynamic characteristics are quasilinear as a function of indicated angle of attack. The calibration also shows Mach number effects in the vane characteristics. The onset of Mach number effects occurs at $M_\infty = 0.90$, where there is a slight nonlinearity in the calibration at indicated angles of attack from 8° to 12°.

The Mach number effect is largest in the transonic region (from $M_\infty = 0.95$ to $M_\infty = 1.30$). At supersonic Mach numbers, the effects of the nose boom on the vanes decreased significantly. These reductions are apparent from Mach numbers of 1.51 to 2.54. At $M_\infty = 2.54$, the effects are almost negligible.

Figure 7 summarizes the angle of attack calibration over the test Mach number range at constant values of angle of sideslip of 0°, 4°, 8°, and 12° and for constant values of angle of attack of 0°, 8°, 16°, and 22°. The angle of attack error curves were obtained from the angle of attack calibration data summarized in appendix B. The curves in figures 7(a) to 7(d) show that the effects of angle of sideslip on angle of attack calibration are negligible. The large increase in the angle of attack errors at Mach numbers near 0.93 were determined to be shock wave effects.

The variation in the vane errors in the supersonic Mach number region at $M_\infty \approx 1.5$ and $M_\infty \approx 2.0$ were also determined to be due to shock interference.
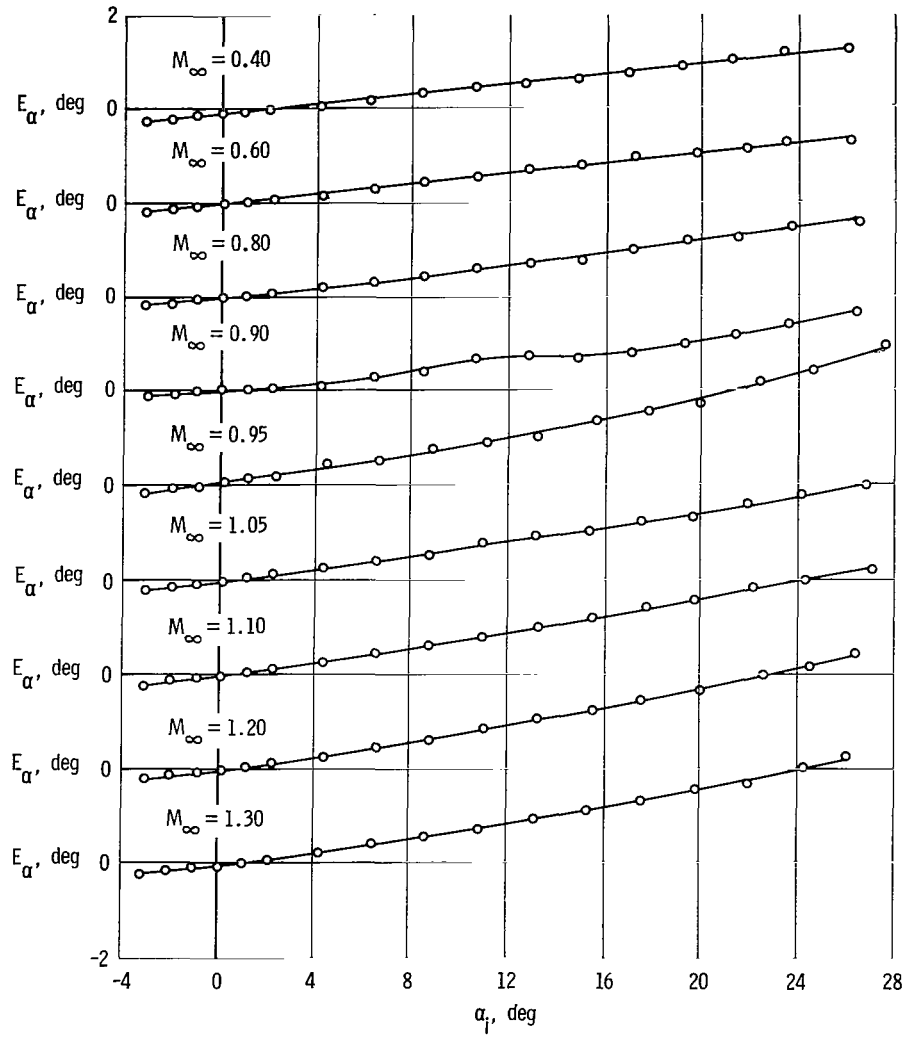
(a)   11-Foot Wind Tunnel.

Figure 6.   Variation in angle of attack vane error at $\beta_t = 0°$.
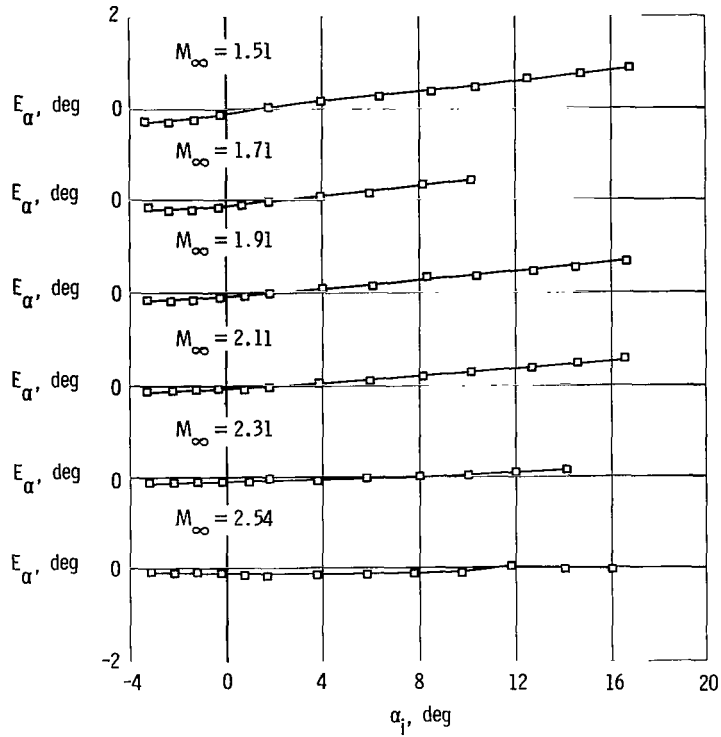
(b) 9- by 7-Foot Wind Tunnel.

Figure 6. Concluded.
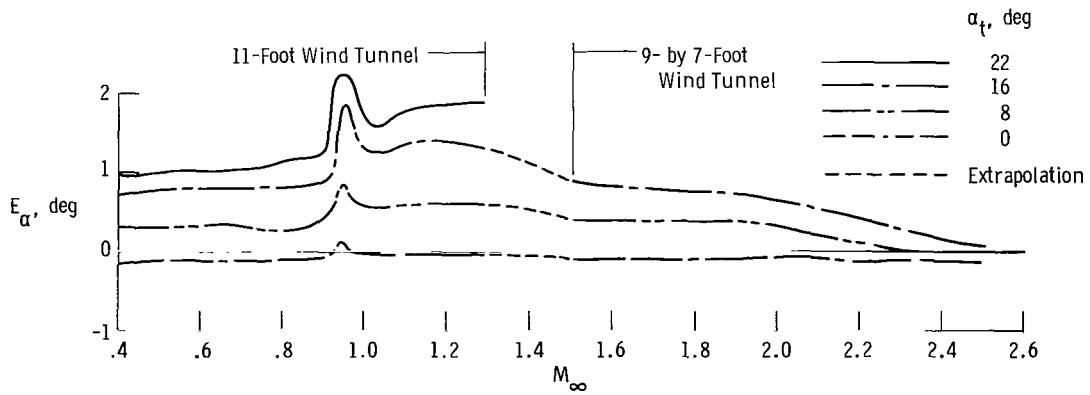
(a) $\beta_i{}^* = 0°$.

Figure 7. Summary of angle of attack vane error
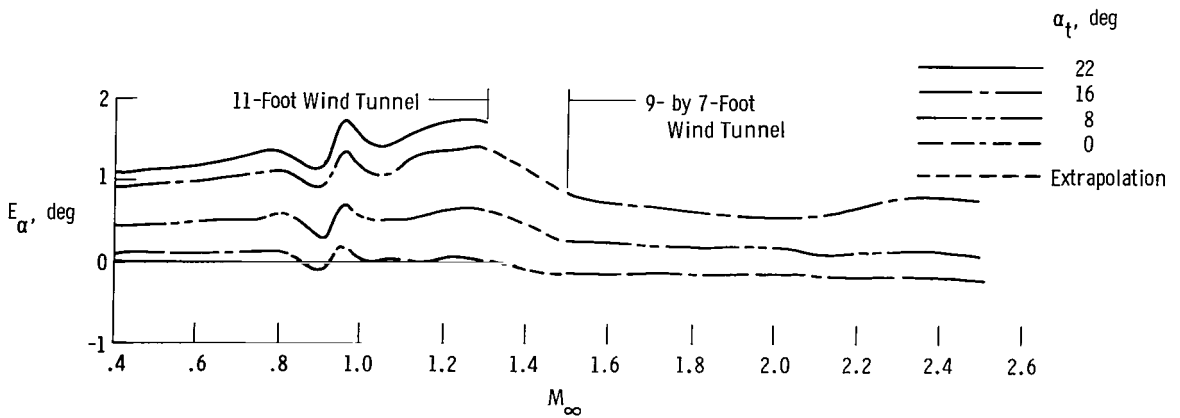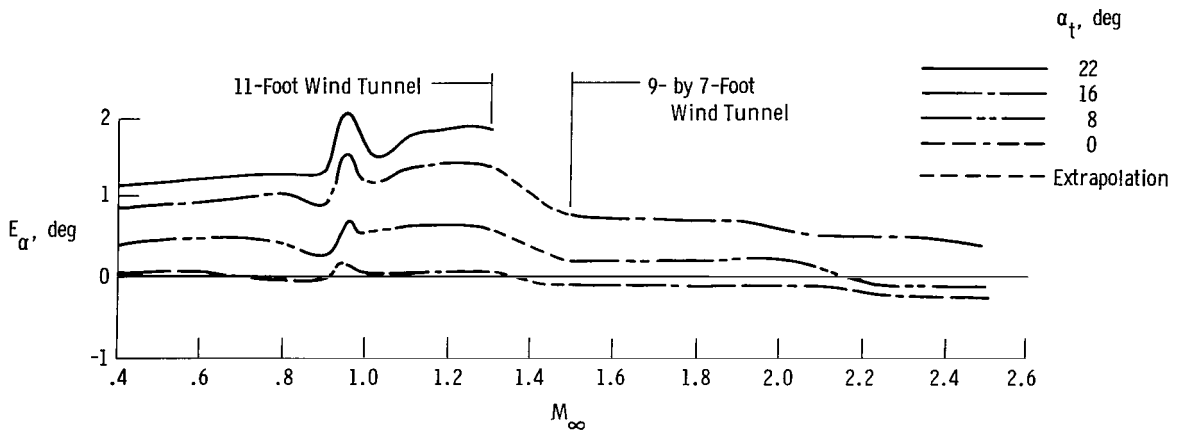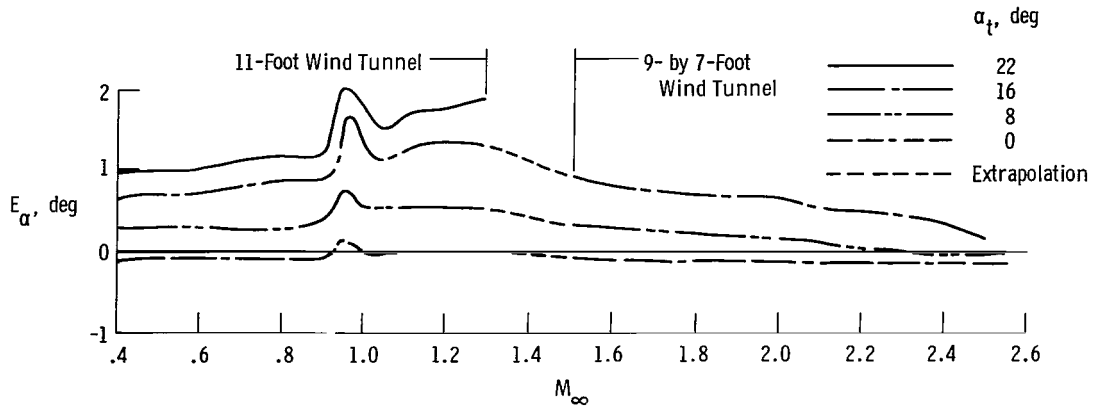at constant angles of attack and sideslip.

11

(b) $\beta_i{}^* = 4°$.

(c) $\beta_i{}^* = 8°$.

(d) $\beta_i{}^* = 12°$.

Figure 7. Concluded.

12

Figure 8 summarizes the angle of attack vane float, $\Delta\alpha_{vf}$, and the nose boom upwash, $\Delta\alpha/\alpha$, from the angle of attack vane calibration curves in figure 6. Vane float (one-half the difference between the upright and inverted indication of the angle of attack vane) represents the float angle of the symmetrically configured angle of attack vane assembly with respect to the left vane centerline. The vane float measurements in figure 8(a) indicate that the angle of attack vanes float approximately ±0.05° trailing edge down (negative angle of attack). The quasilinearity of the vane calibration in figure 6 makes it possible to define aerodynamic upwash in terms of $\Delta\alpha/\alpha$ (fig. 8(b)). In this form upwash can be shown as a function of Mach number with $\beta_t = 0°$, a form which is amenable to comparison with predictions. The error due to upwash contains shock interference effects at transonic and supersonic speeds.
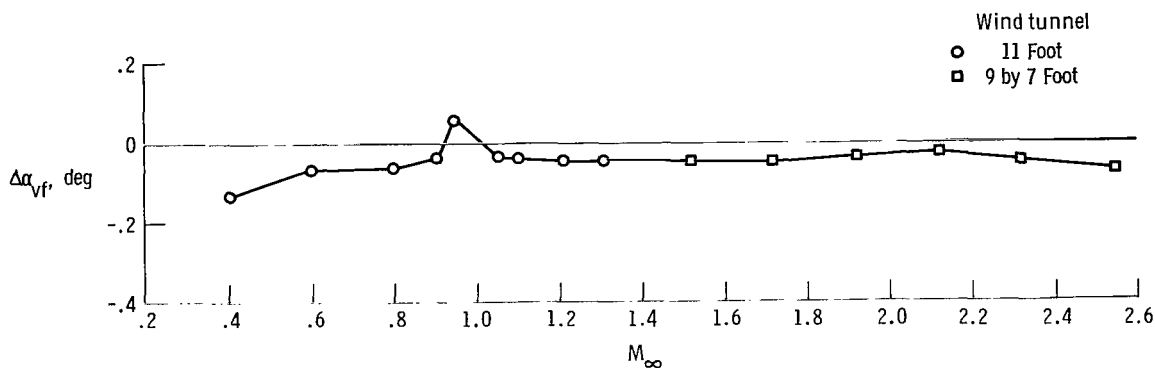
(a) Vane float.
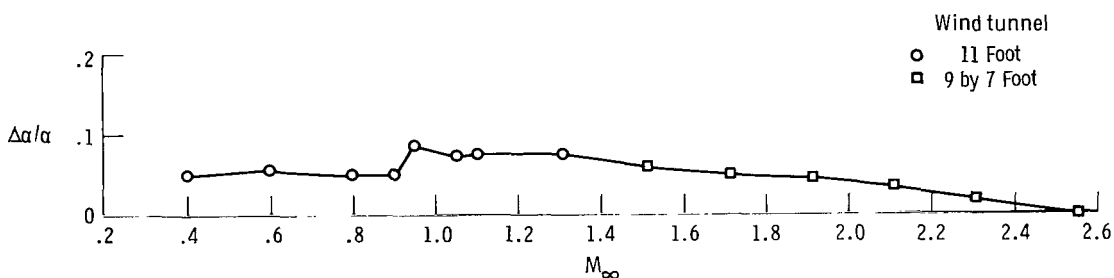
(b) Nose boom upwash.

Figure 8. Variation of vane float and nose boom upwash in the angle of attack vane at $\beta_t = 0°$.

Angle of sideslip calibration data. - Figure 9 summarizes the angle of sideslip vane calibration at a zero angle of attack ($\alpha_t = 0°$) for the Mach numbers tested. The calibration shows the aerodynamic characteristics of the vane in terms of vane position error (E_β). Like the angle of attack vane calibration, the angle of sideslip vane

calibration shows vane float, nose boom sidewash, and Mach number effects. The variations in the calibration are quasilinear with angle of sideslip except for Mach numbers above 1.50. Above $M_\infty = 1.50$, the calibrations are highly nonlinear, with error reversals which were determined to be the effect of shock interference with the vane.
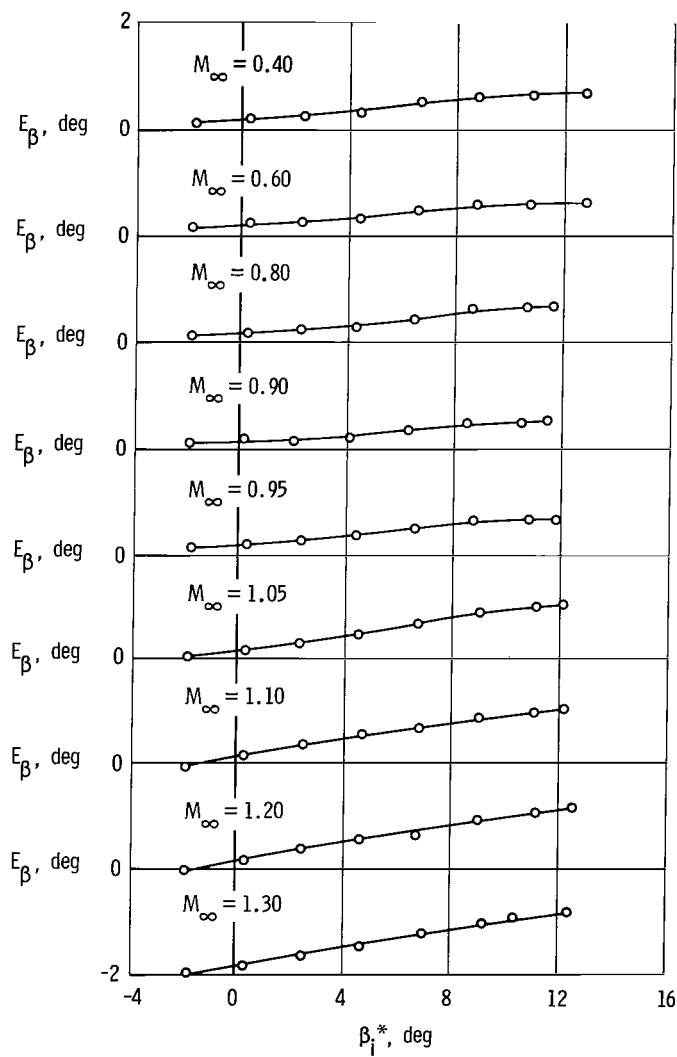
(a) 11-Foot Wind Tunnel.

Figure 9. Variation in angle of sideslip vane error at $\alpha_t = 0°$.
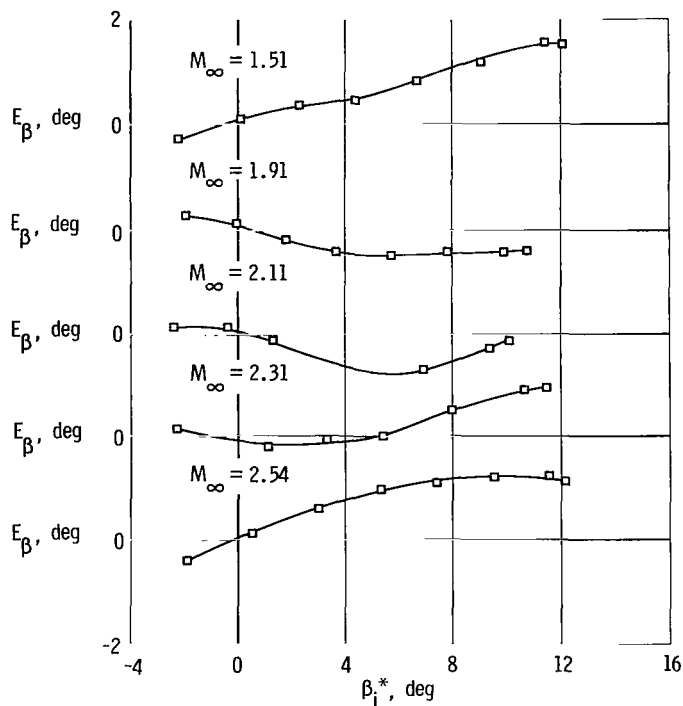
(b) 9- by 7-Foot Wind Tunnel.

Figure 9. Concluded.

Figure 10 summarizes the angle of sideslip over the test Mach number range at constant values of angle of attack (0°, 8°, 16°, and 24°) and for constant values of angle of sideslip (0°, 4°, 8°, and 12°). The angle of sideslip vane error curves were obtained from the angle of sideslip calibration summarized in appendix B. The variations in the data in figure 10(a) show the extent of the Mach number effects beginning at $M_\infty \approx 1.50$. The interference effects are greatest at sideslip angles other than zero. Figures 10(b) to 10(d) show that as angle of attack increases the Mach number for the onset of shock interference decreases.
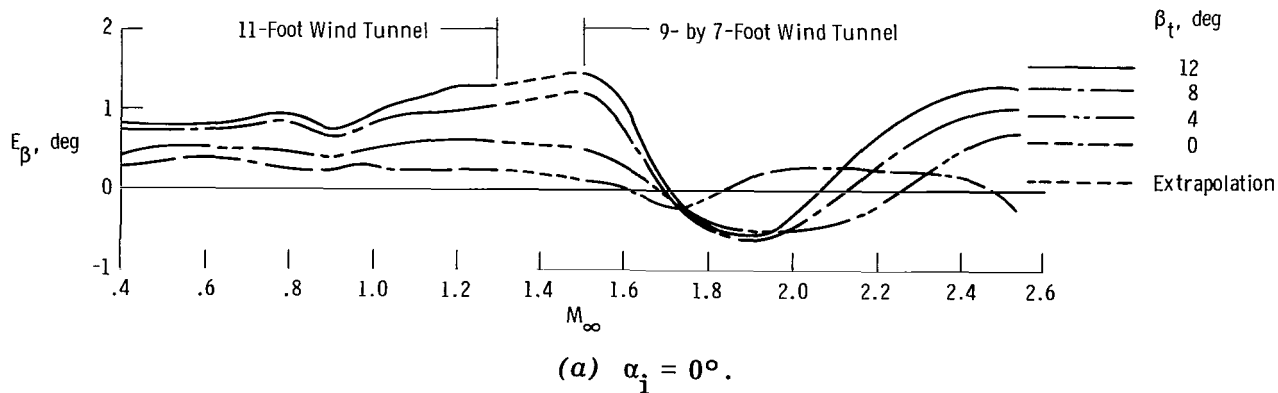
(a) $\alpha_i = 0°$.

Figure 10. Summary of angle of sideslip vane error at constant angles of attack and sideslip.

15
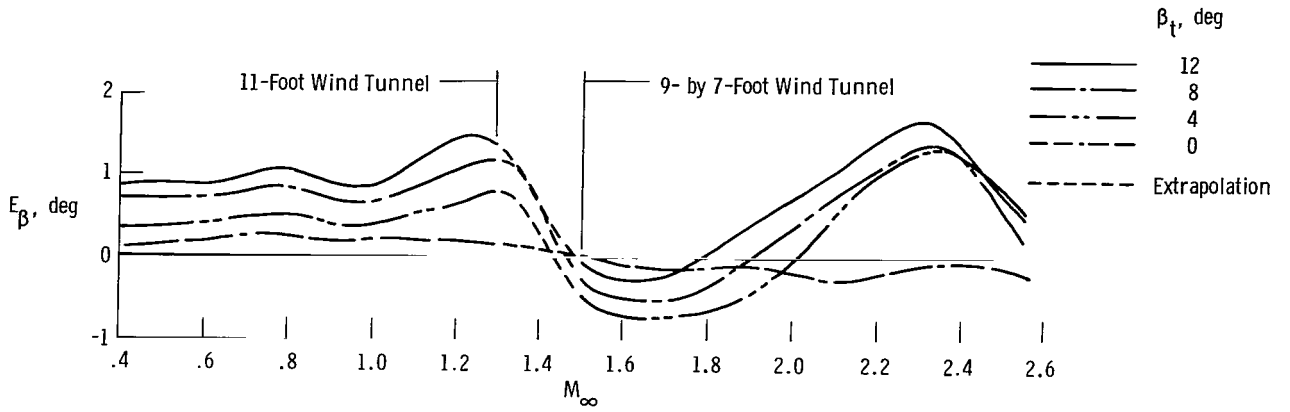
(b) $\alpha_i = 8°$.
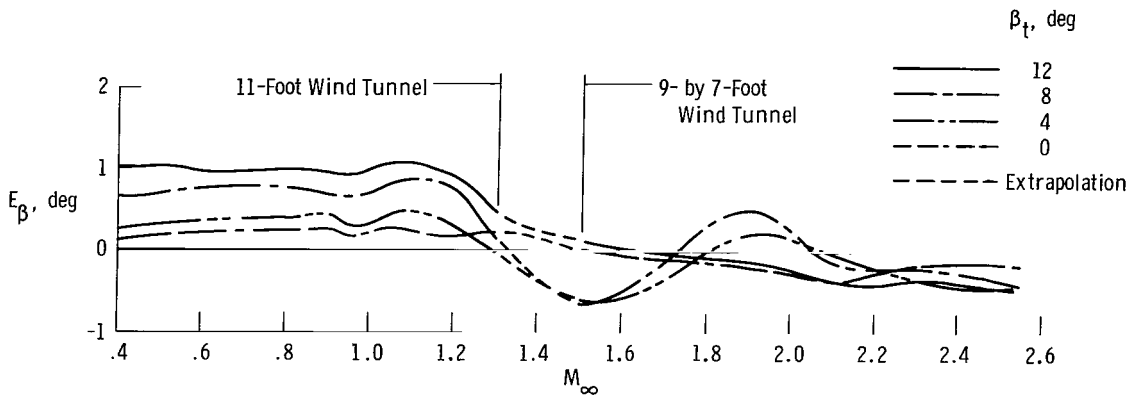
(c) $\alpha_i = 16°$.
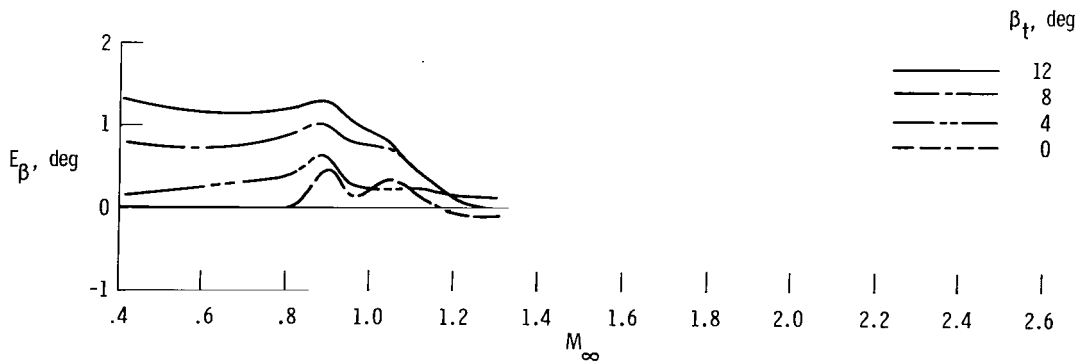
(d) $\alpha_i = 24°$.

Figure 10. Concluded.

16

Figure 11 summarizes the vane float, $\Delta\beta_{vf}$, and the aerodynamic sidewash of the angle of sideslip vane calibration in figure 9 in terms of $\Delta\beta/\beta$. The vane float values for the angle of sideslip vane in figure 11(a) were also obtained from upright and inverted tests. The vane floated less than 0.20° trailing vane left (positive angle of sideslip). The apparent discontinuity between the vane float values from the 11-Foot and the 9- by 7-Foot Tunnels at Mach numbers of 1.3 and 1.5 may be due to a misalinement in the angle of sideslip plane in the 11-Foot Tunnel. The angle of sideslip vane sidewash is summarized in figure 11(b) in terms of $\Delta\beta/\beta$ over the Mach number range. The sidewash was calculated from only the quasilinear portions of the calibrations in figure 9. For supersonic Mach numbers, for which the angle of sideslip calibrations were highly nonlinear, only the linear portions of the calibration curves (the portions near the origin) were used. Even so, the effects of Mach number on sidewash were large at Mach numbers above 1.50.
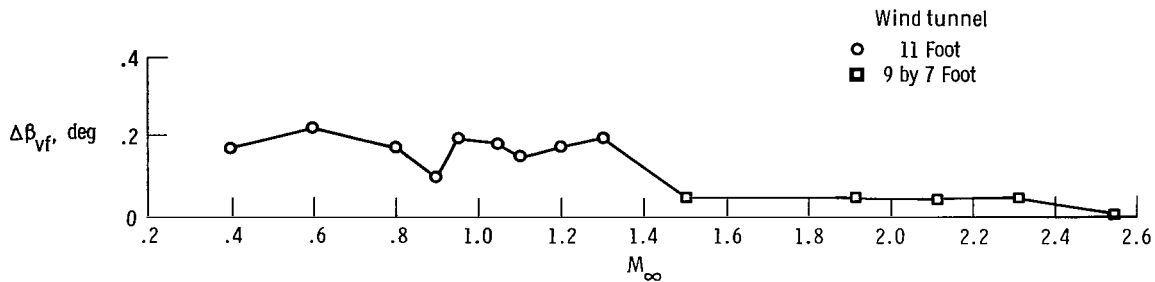
(a) Vane float.
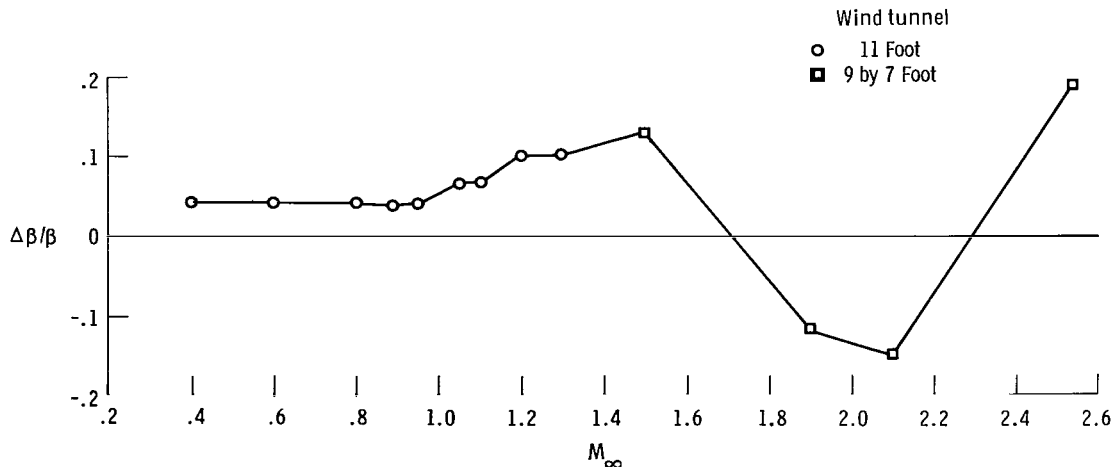
(b) Nose boom sidewash.

Figure 11. Variation of angle of sideslip vane
vane float and nose boom sidewash at $\alpha_t = 0°$.

Unit Reynolds number effects. - Tests were conducted on the test installation at Mach numbers of 0.90, 1.30, and 1.51 to determine the effects of Reynolds number on the vane error. Reynolds number ranged from 6.6×10^6 per meter (2.0×10^6 per

foot) to 18.0 $\times$ 10^6 per meter (5.5 $\times$ 10^6 per foot). The effects of Reynolds number were determined to be negligible.

Flow field description. - A series of tests was performed for the purpose of flow visualization in order to better define the influence of the local flow field on the vane assemblies. Schlieren photographs were taken over the Mach number range from 0.70 to 2.54. For the Mach number range from 0.70 to 1.15, Schlieren photographs were taken at zero angles of attack and sideslip only. Above a Mach number of 1.15, Schlieren photographs were also taken at other combinations of angle of attack and angle of sideslip; angle of attack varied up to 16° and angle of sideslip varied up to 10°.

In the transonic Mach number region, the Schlieren photographs showed that flow was supercritical about the vane assemblies at free stream Mach numbers above approximately 0.85. The supercritical condition appeared in the Schlieren photographs as local shock formations near the angle of attack and angle of sideslip vane assemblies. Figure 12 is a Schlieren photograph of the flow angularity sensor portion of the test installation at M_∞ = 0.95 and zero angles of attack and sideslip and shows the positions of these shock formations. One is to the rear of the angle of attack vane and the other is at the angle of sideslip vane. This supercritical condition is attributed to the size of the section of the sensor between the pitot-static probe and the angle of attack vane assembly. This section of the vane housing has an outside diameter of 8.25 centimeters (3.25 inches), compared with the 1.91-centimeter (0.75-inch) outside diameter of the section of the boom housing the pitot-static probe system. Local shock formation was also observed at the pitot-static probe tip due to the small tip expansion. Sketches of the sensor showing the development of these weak shock formations and their passage downstream of the vane assemblies are presented in figure 13 for the Mach number range from 0.85 to 1.10.
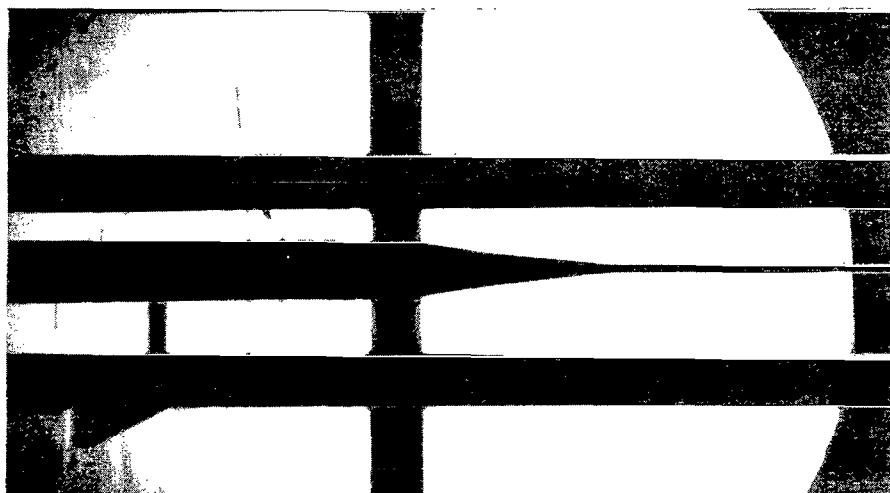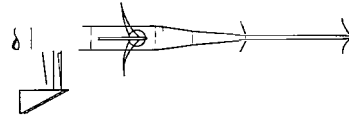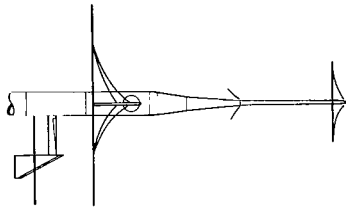

Figure 12. Photograph of flow angularity sensor at M_∞ = 0.95. α_t = 0°; β_t = 0°.
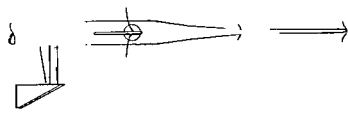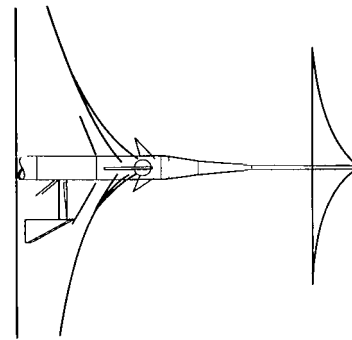
(a) $M_\infty = 0.85$.
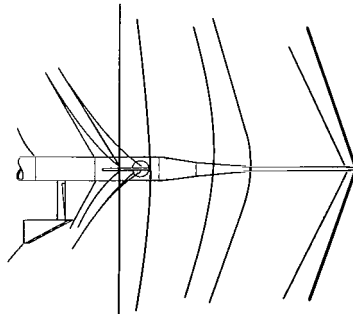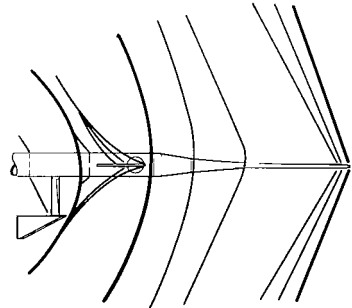
(b) $M_\infty = 0.90$.

(c) $M_\infty = 0.95$.

(d) $M_\infty = 1.00$.

(e) $M_\infty = 1.05$.

(f) $M_\infty = 1.10$.

Figure 13. Sketches of shock patterns about flow angularity sensor at zero angles of attack and sideslip in transonic flow.

19

In the angle of attack data obtained during the Schlieren tests and summarized in figure 14 (which shows the $\alpha_t = 0°$ data from figure 7(a)), the data variation at $M_\infty \approx 0.93$ is believed to be due to local shock wave formations about the angle of attack vanes in combination with the effects of the angle of sideslip vane pressure field. The sketches for $M_\infty = 0.90$ and $M_\infty = 0.95$ (figs. 13(b) and 13(c)) show that the local shock originating at the angle of attack vanes moves from the post's leading edge to the trailing edge of the angle of attack vanes. The adjustment of the shock to a position behind the vanes may have isolated the angle of attack vanes from the pressure field effect at the higher Mach numbers.
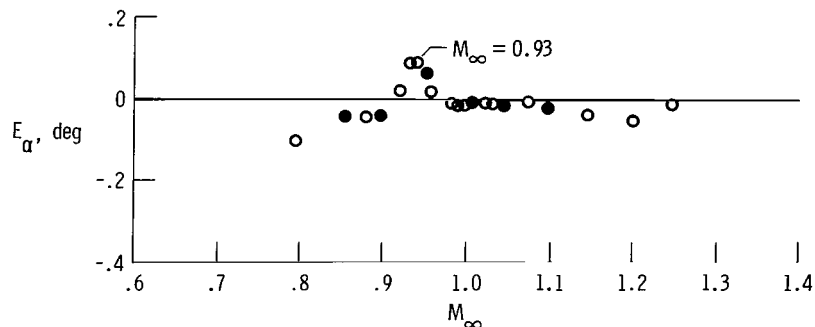
Figure 14. Variation of angle of attack vane error obtained during Schlieren tests of flow angularity sensor at zero angles of attack and sideslip. Solid symbols denote conditions shown in figure 13.

The effects of the local shock formation generated at the angle of attack vane assembly appear to be more significant as the test installation is displaced in angle of attack and angle of sideslip. The strength of the shock and the relative position between the shock and the vanes change with the changing angles. These changes are reflected particularly in the calibration data in figures 7 and 10 at transonic Mach numbers near 0.95. No Schlieren photographs are available at other than the zero angle of attack and sideslip condition to show the position changes of these shock formations. Schlieren photographs did not indicate any shock interference effects on the angle of attack vane from the angle of sideslip vane between $M_\infty = 0.95$ and $M_\infty = 1.30$, where the large transonic error is observed in the angle of attack vane calibration data in figures 6 and 7. An evaluation of the present test configurations without the angle of sideslip vane assembly was beyond the scope of the calibration tests. Further developmental tests on the test configuration may resolve the large transonic errors.

Schlieren photographs of the angle of attack and angle of sideslip vanes obtained at supersonic Mach numbers showed that shock waves impinged on the vane assemblies at approximately the Mach numbers at which large variations appeared in the calibration data in figures 7 and 10. Figure 15 shows a sketch of a Schlieren photograph taken at $M_\infty = 1.30$ and at zero angles of attack and sideslip. The sketch identifies the various shock systems generated locally over the sensor. Mach lines
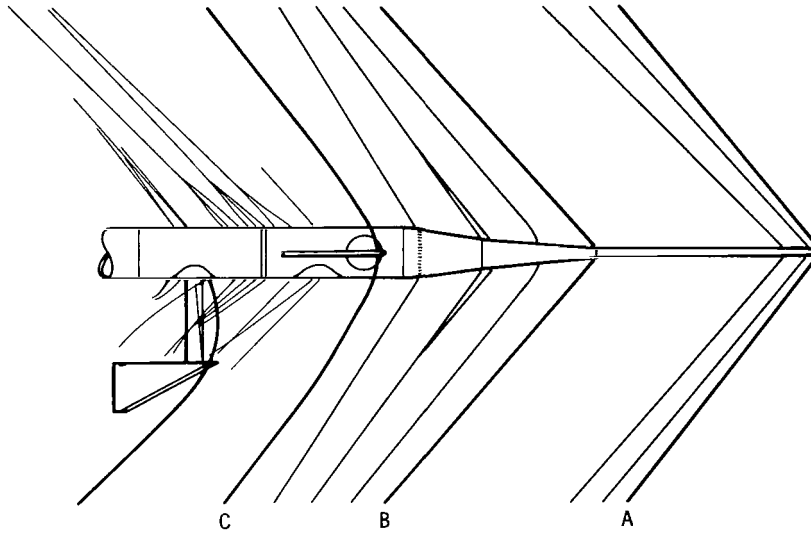
20

Figure 15. Sketch of Schlieren photograph showing various shock systems about flow angularity sensor. $M_\infty = 1.30$; $\alpha_t = 0°$; $\beta_t = 0°$.

were constructed for the shocks identified as A, B, and C to determine the position of these shocks along the vane post centerline. The results are summarized in figure 16 for zero angles of attack and sideslip in terms of a ratio of the radial distance from the shock wave to the vane center of pressure, R'/R. In figure 16, the crosshatched areas show the Mach number range in which a shock interferes with the vanes (shock B for the angle of attack vanes and shock C for the angle of sideslip vane). These interference effects are reflected in the variation of the angle of attack vane calibration data for Mach numbers above 2.0 in figure 7(a) for $\alpha_t = 0°$ and in the angle of sideslip vane calibration data for Mach numbers between 1.6 and 2.2 in figure 10(a) for $\beta_t = 0°$. Figure 16 also shows that any displacement of the test installation from zero in either of the two axes can position the vanes into the shocks at Mach numbers below the interference Mach numbers for zero angles of attack and sideslip. These interference effects are apparent in the variations in the angle of attack calibration data in figures 7(a) to 7(d) at Mach numbers from approximately 1.3 to 1.5 and in the variations in the angle of sideslip calibration data in figures 10(a) to 10(d) at Mach numbers from approximately 1.0 to 1.5. The variations in the angle of sideslip data in figures 10(b) and 10(c) indicate that the angle of sideslip vane is also influenced by an additional shock system. From the shock position variation in figure 16 it appears that the interference is due to a shock from the boom expansion section (shock system B).
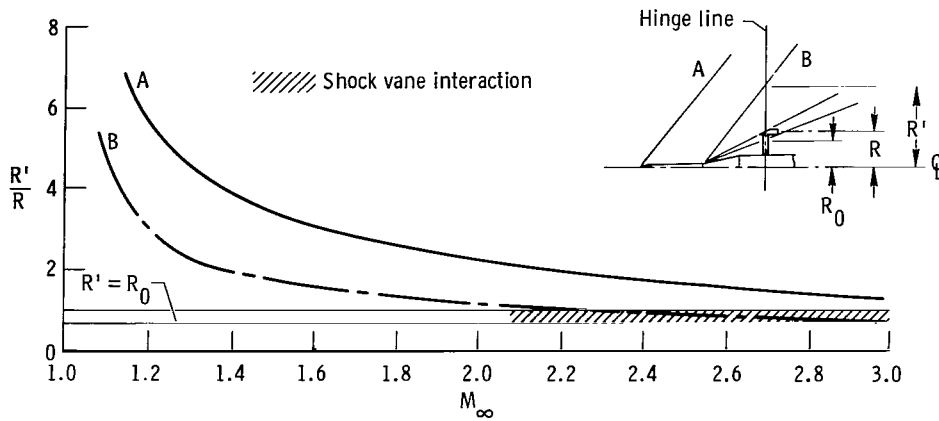
(a) Angle of attack vane.
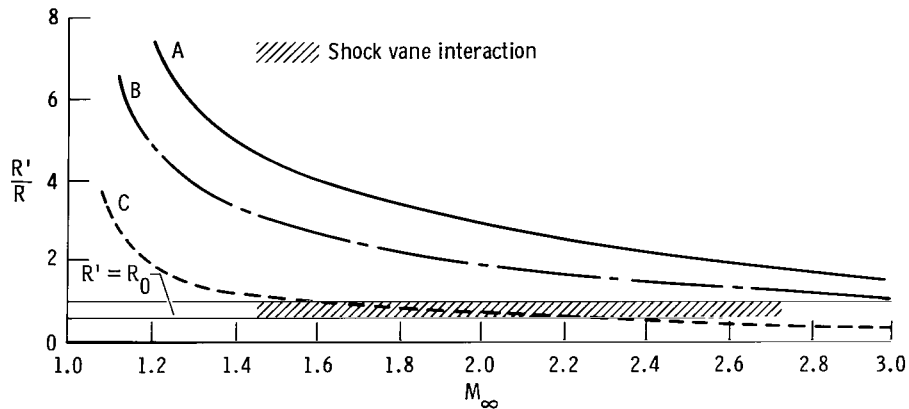
(b) Angle of sideslip vane.

Figure 16. Summary of shock position along angle of attack
and angle of sideslip post hinge line. $\alpha_t = 0°$; $\beta_t = 0°$.

Comparisons of Flow Angularity Sensor Systems

Two types of comparisons were made. First, the calibration data from these tests were compared with the previous test results (refs. 4 to 6). The purpose of the comparison was to assess the effects of configuration changes on the vanes' aerodynamic characteristics and to augment the previous test results. Second, the calibration data for the system described in reference 4 were compared with the calibration data for the NACA system described in reference 3. The purpose of the comparison was to identify aerodynamic similarities between the two dissimilar flow angularity vanes.

22

In the first comparison, the system described in reference 4 was tested with the post for the angle of sideslip vane assembly located under the angle of attack vane center of pressure. The tests of this configuration covered a Mach number range from 0.2 to 3.0 and resulted in calibration data for both the angle of attack and angle of sideslip vanes. The system described in references 5 and 6 was similar to the system described in reference 4 except that the angle of sideslip vane assembly was 15.95 centimeters (6.28 inches) farther rearwards. Reference 5 contains angle of attack and angle of sideslip vane calibration results for Mach numbers up to 1.3. Reference 6 contains angle of sideslip vane calibration results for Mach numbers from 1.5 to 3.0. The configuration used in the present tests was like that in references 5 and 6; that is, the angle of sideslip vane assembly was 15.95 centimeters (6.28 inches) rearwards of the angle of attack vane assembly. However, a slightly different pitot-static probe installation was employed for the measurement of total and static pressures, and this entailed the use of a different expansion section in front of the angle of attack and angle of sideslip vanes and a slightly different pitot head shape.

In the second comparison, which was between the systems described in references 3 and 4, the locations of the angle of attack and angle of sideslip vane assemblies were the same. The two systems represent radically different designs, however. The diameter of the boom housing to which the reference 4 (and present test) vanes were attached was approximately twice the diameter of the housing for the NACA system. The flow angularity vanes of the reference 4 system (identical to the vanes in fig. 3) were flat plates which were swept and beveled at the leading edge and were fixed to a rotating aerodynamically contoured post. Furthermore, the angle of attack vane assembly was dual vaned and symmetrically arranged. This design was different from the NACA design (fig. 17, from ref. 3), in which the vanes were thin, low-aspect-ratio flat plates which rotated about a fixed cylindrical post. In the NACA system, a free air temperature sensor was installed diametrically opposite the angle of attack vane to preserve planform symmetry. Both systems employed a single angle of sideslip vane located under the angle of attack vane assembly.
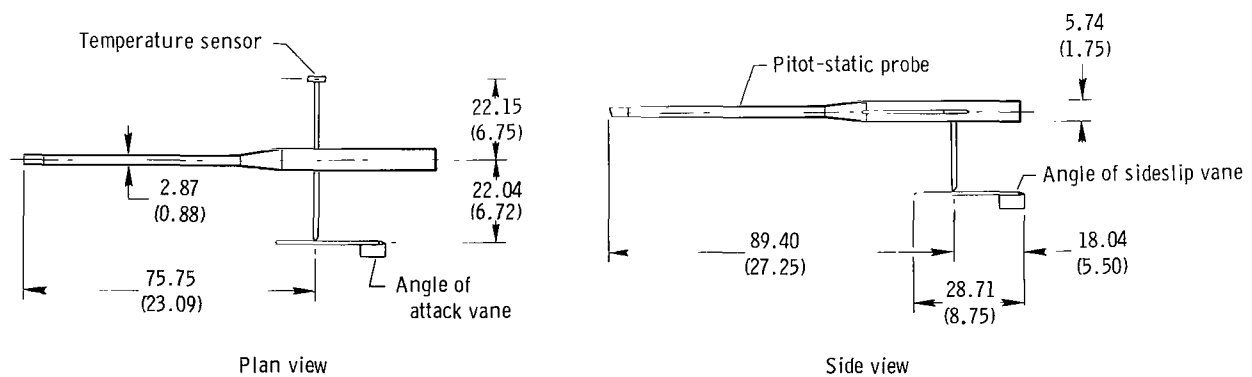
Figure 17. NACA flow angularity sensor (ref. 3).
Dimensions are in centimeters (inches).

Comparisons with previous AEDC calibrations. – Figure 18 compares the angle of attack calibration data obtained during this study with the calibration data obtained for the systems described in references 4 and 5. The figure shows variations in the calibration for the angle of attack vane at $\beta_t = 0°$ and at $\alpha_t = 0°$, $10°$, and $20°$ over the Mach number range tested. The error is large in the transonic Mach number region for the reference 4 data. This error was determined to be due to shock interference from the angle of sideslip vane and precipitated the reference 5 tests. In the reference 5 system, the angle of sideslip vane was moved rearwards 15.95 centimeters (6.28 inches), and this appears to have prevented the shock produced by the angle of sideslip vane from interfering with the angle of attack vanes. However, the effects of shock interference are still apparent in the data for the present test configuration, although at a lower level and in a narrow Mach number band centered on $M_\infty = 0.95$. These shock interference effects were determined in the preceding discussion to be the influence of adjustments to the locally generated shock about the angle of attack vane in combination with the effects of the pressure field effect around the angle of sideslip vane. The influence of the angle of sideslip vane on the angle of attack vanes appears to be minimized by installing the angle of sideslip vane in the rear position. Except for this difference at transonic Mach numbers, the present calibration verifies the reference 5 calibration. The differences between the pitot-static probe systems in reference 5 and the present study did not significantly alter the angle of attack vane calibration.

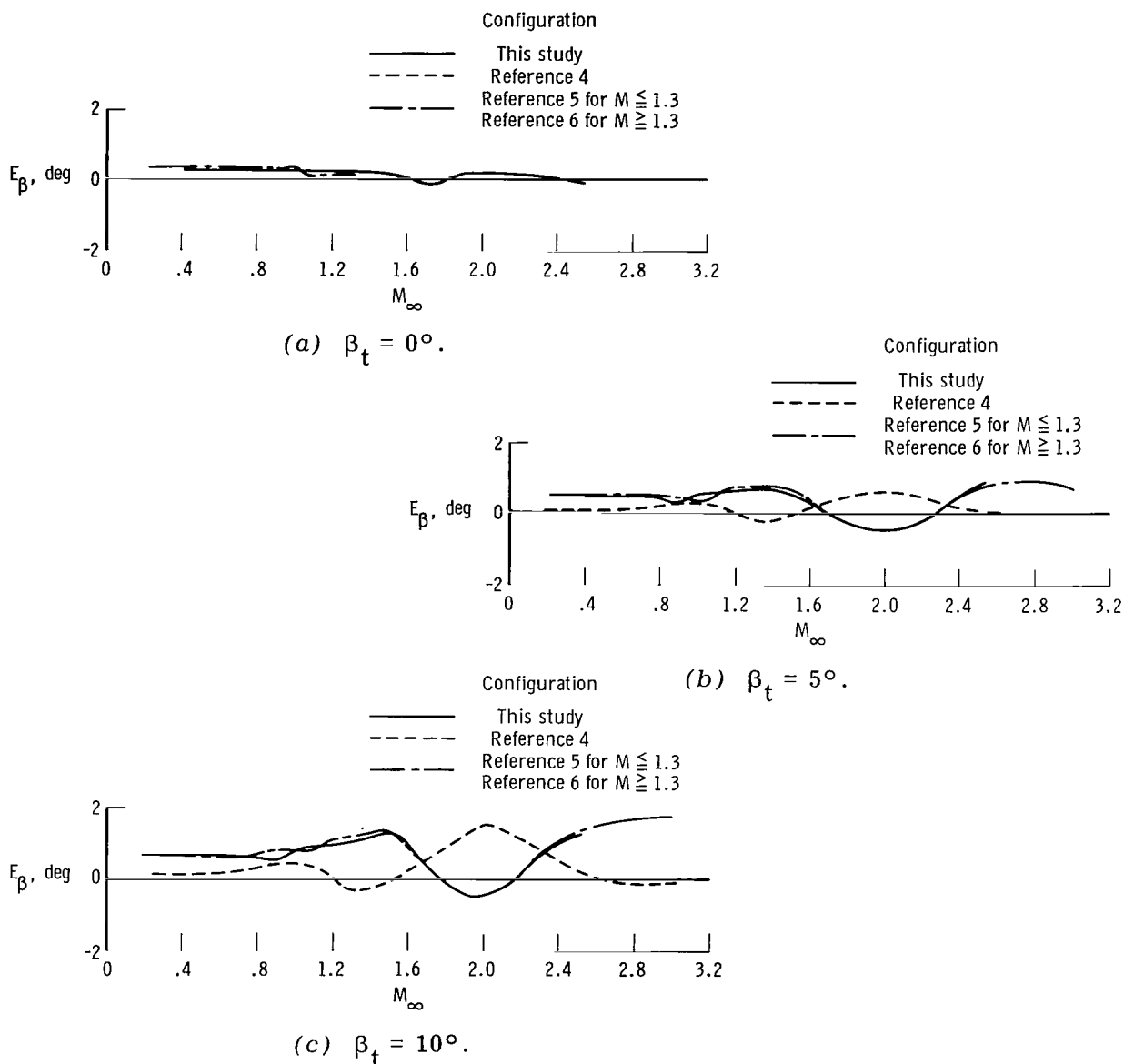(a) $\alpha_t = 0°$.

(b) $\alpha_t = 10°$.

(c) $\alpha_t = 20°$.
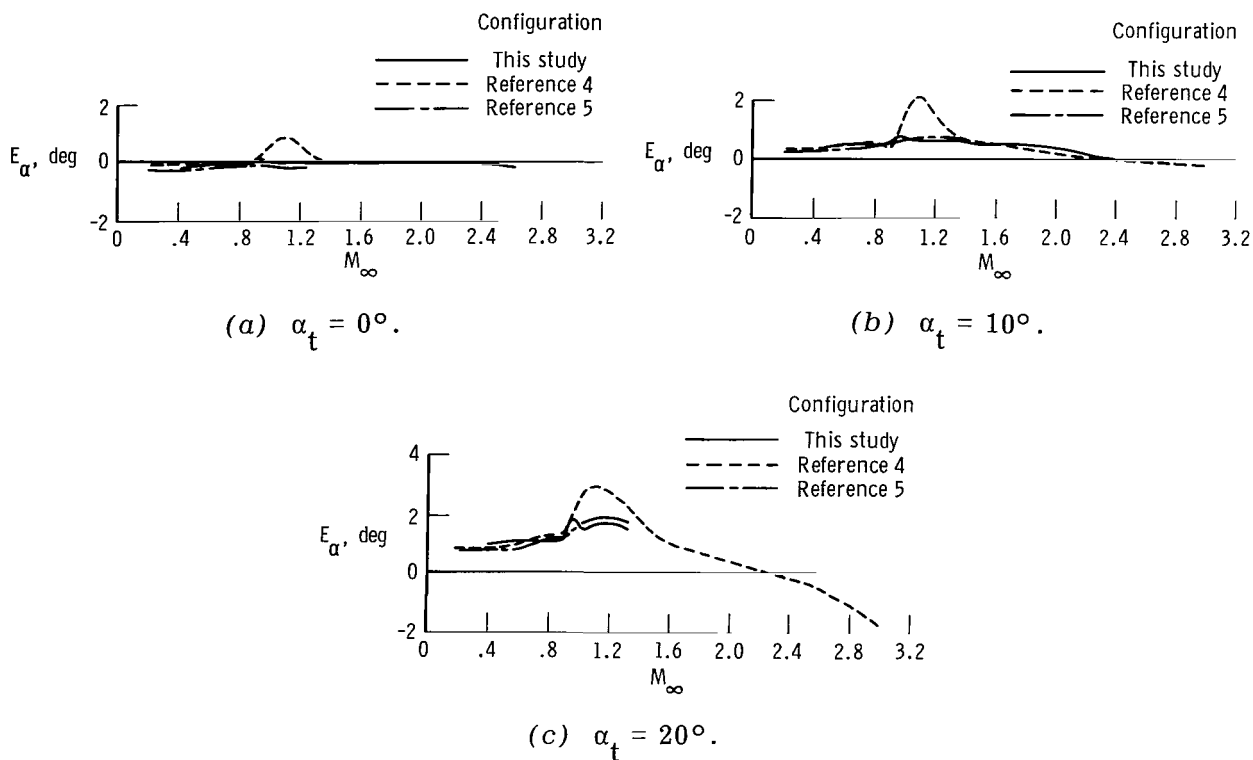
Figure 18. Comparison of angle of attack vane error for present and previous tests. $\beta_t = 0°$.

24

Figure 19 compares the angle of sideslip vane calibration results for this study with those for the systems in references 4 to 6 at $\alpha_t = 0°$ and at $\beta_t = 0°$, $5°$, and $10°$. The comparison shows that the forward location of the angle of sideslip vane in reference 4 appears to have kept error near zero for subsonic Mach numbers (up to 0.8) while allowing the early onset of shock interference transonically ($M_\infty = 0.8$ to 1.2) and supersonically ($M_\infty = 2.0$). Moving the angle of sideslip vane back delayed the onset of shock interference to a higher Mach number but introduced an error at subsonic Mach numbers. The data from the present tests are in excellent agreement with the data from references 5 and 6 over the entire Mach number range.

(a) $\beta_t = 0°$.

(b) $\beta_t = 5°$.

(c) $\beta_t = 10°$.

Figure 19. Comparison of angle of sideslip vane error for present and previous tests. $\alpha_t = 0°$.

Comparison with a NACA configuration. - The calibration data from references 3 and 4 at $\beta_t = 0°$ and at $\alpha_t = 0°$, $10°$, and $20°$ are compared in figure 20. The data show that even though the vane designs were different, the aerodynamic characteristics of the angle of attack vane assemblies were similar. In both vane configurations the angle of sideslip vane was under the angle of attack vane, and both configurations show large transonic errors over nearly the same transonic Mach number range. The variations in figure 20 suggest that the angle of attack vane error may be independent of vane configuration at moderate angles of attack and dependent instead on variations in local flow conditions about the vanes.
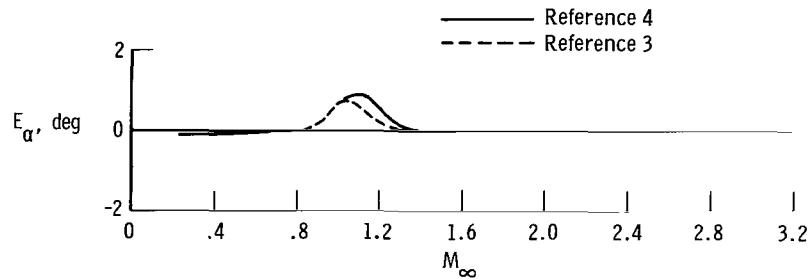
(a) $\alpha_t = 0°$.
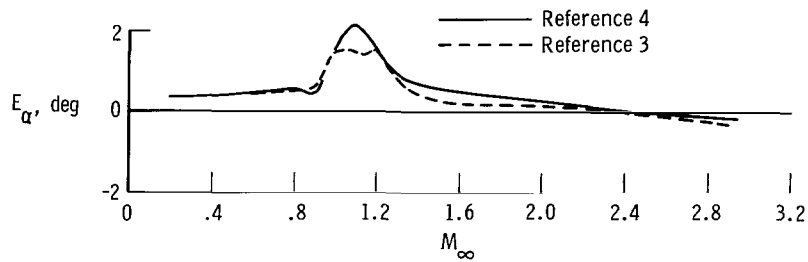
(b) $\alpha_t = 10°$.
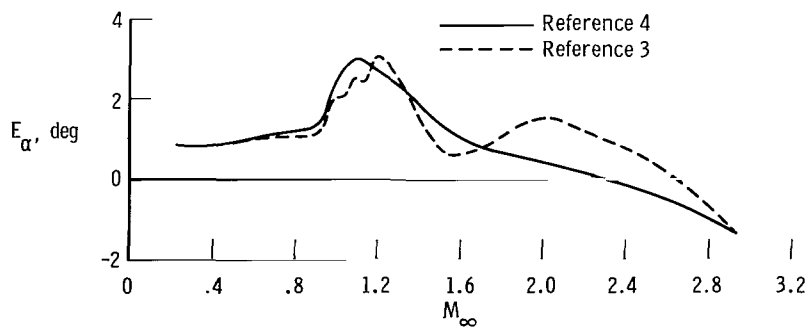
(c) $\alpha_t = 20°$.

Figure 20. Comparison of angle of attack vane error at $\beta_t = 0°$ for reference 4 and NACA vane configurations. Angle of sideslip post locations are identical.

When the angle of sideslip vane calibration for the two systems are compared (fig. 21), the data show similar variations over the Mach number range. Both systems show approximately zero error subsonically. The configuration with the angle of sideslip vane under the angle of attack vane appears to be best for this Mach number range, since no correction to sideslip is necessary. The transonic and supersonic variations are due to shock interference. The shock interference onset Mach numbers for the two systems are comparable. The comparison suggests that the aerodynamic variations for the angle of sideslip vane may also be due to local flow rather than vane configuration.
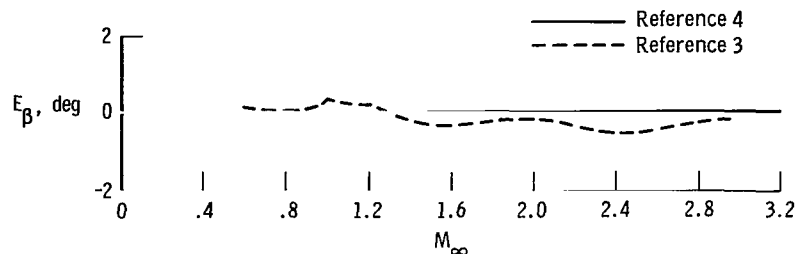
(a) $\beta_t = 0°$.
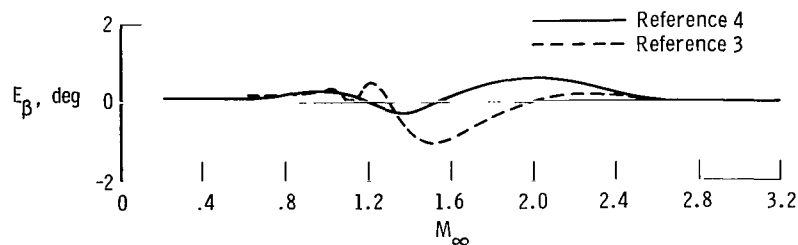
(b) $\beta_t = 5°$.
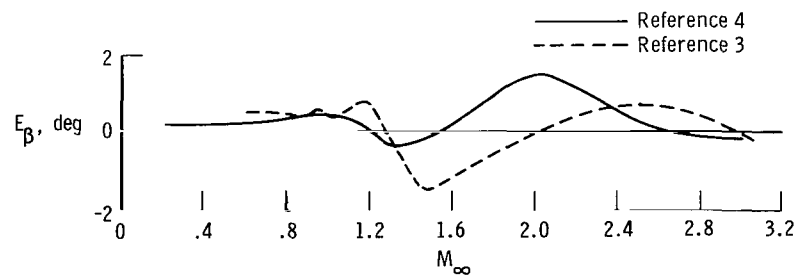
(c) $\beta_t = 10°$.

Figure 21. Comparison of angle of sideslip vane error at $\alpha_t = 0°$ for reference 4 and NACA vane configurations. Angle of sideslip post locations are identical.

The comparisons in figures 20 and 21 show the reference 4 configuration and the NACA configuration (ref. 3) to have similar aerodynamic characteristics. However, the natural frequency and damping of the test type of vane are approximately one-half those of the NACA vane. Figure 22 compares the natural frequency and damping data for the two systems. The reference 3 data are compared with previously unpublished data from the NASA Flight Research Center and the Air Force Flight Test Center at Edwards, Calif. The low dynamic characteristics exhibited by the test type of vane are attributed to the coupling of the large vane assembly with the mass of the flightpath accelerometer units attached to the shaft.
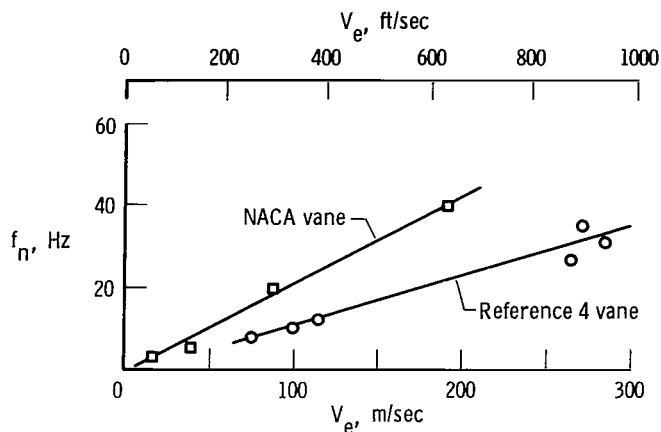
(a) Natural frequency.
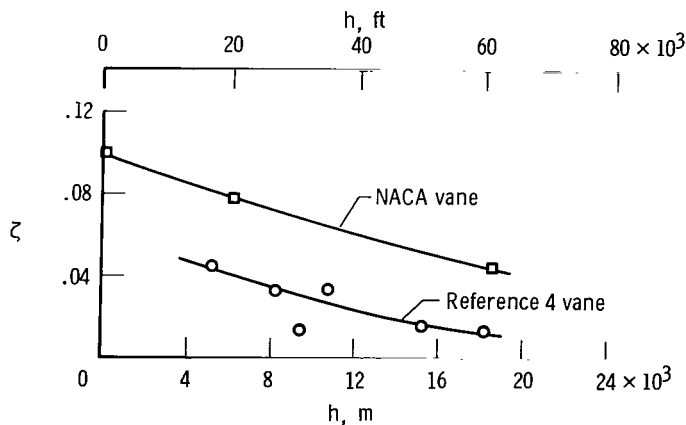
(b) Damping ratio.

Figure 22. Comparison of dynamic characteristics of test type of vane and NACA vanes.

Comparison Between Wind Tunnel and Analytical Predictions

Analytical predictions that estimate the effects of the upwash on nose boom-mounted vanes are of considerable interest for full-scale flight testing. For boom-vane systems mounted on aircraft, the upwash prediction technique described in reference 10 in conjunction with the technique described in reference 11 is widely used. For boom-vane systems alone, the configuration can be treated as a wing-body, and the prediction technique outlined in reference 12 can be used. When viewed as a wing-body configuration, the results of prediction techniques in references 10 and 12 are essentially the same at zero Mach number.

The nose boom upwash estimate computed by the reference 10 technique for the nose boom installation in figure 5 is presented in terms of $\Delta\alpha/\alpha$ for zero Mach number in figure 23. Agreement is reasonably good between this prediction and the wind tunnel measurements for subsonic speeds. The error for the entire Mach number range can be approximated by using the value predicted for zero Mach number.
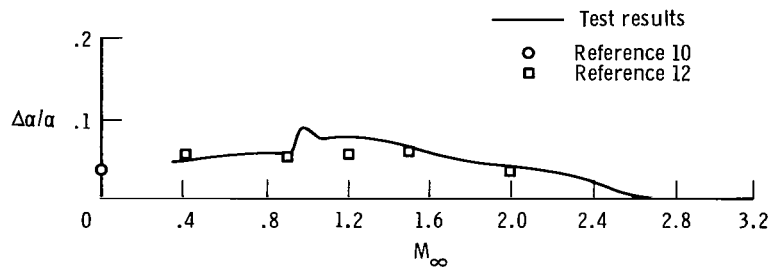
Figure 23. Comparison between wind tunnel and analytical predictions of effects of upwash on angle of attack vanes for test installation (nose boom only).

The upwash predictions made by the reference 12 method for selected Mach numbers from 0.4 to 2.0 are also presented in figure 23. This method shows reasonably good agreement with the wind tunnel-derived values of upwash over the entire Mach number range and account for the diminishing effect of Mach number at supersonic speeds. However, the analytical predictions do not account for shock-to-vane interaction effects observed in the wind tunnel data.

CONCLUSIONS

A wind tunnel investigation was conducted on a vane flow angularity sensor system capable of measuring flightpath accelerations in an attempt to define the aerodynamic characteristics of the flow angularity vanes. The flow angularity calibration is summarized and discussed. The data are compared with wind tunnel data for other vane flow angularity systems and also with analytical predictions. The

following conclusions were drawn from the study:

1. The angle of attack and angle of sideslip vanes both showed errors throughout the Mach number range tested for all angles of attack and angles of sideslip. The errors were due to the influence of the nose boom on the vanes at all displacements of the nose boom assembly.

2. The angle of attack and angle of sideslip calibrations both showed that the most significant effects on the vane error were due to Mach number. The Mach number effects, which resulted in nonlinearities, were determined to be due to shock wave interference effects on the vane assemblies. The Mach number effects on the angle of attack vanes at the low transonic Mach numbers were due to adjustments of the locally generated shock formations about the vanes. The Mach number effects for the angle of attack and angle of sideslip vanes in the high transonic and supersonic Mach number range were determined to be shock-to-vane interaction effects from shock waves generated immediately upstream of the vane assemblies.

3. The variations due to Mach number in the transonic angle of attack calibration and the supersonic angle of sideslip calibration suggest that the angle of sideslip vane may be too near the angle of attack vane.

4. The effect of angle of sideslip on the angle of attack calibration is negligible. The effect of angle of attack on the angle of sideslip calibration is significant, the effect being to reduce the onset Mach number for the shock interference.

5. Two significantly dissimilar vane configurations, the test type of vane and a standard NACA vane, showed similar aerodynamic characteristics over the entire Mach number range up to moderate angles of attack. This similarity suggests that the aerodynamic characteristics are independent of the type of vane configuration and dependent instead on the effect of the boom housing on the vanes and on the distance between the vane assemblies.

6. The frequency and damping of the test type of vane are approximately one-half those of a NACA vane.

7. Analytical prediction techniques provided reasonable estimates of nose boom upwash at zero Mach number and over the entire Mach number range tested. The prediction method does not account for the effects of shock-to-vane interactions on the wind tunnel data.

8. The calibration results reported herein verify and extend previous wind tunnel results for a similar configuration.

Flight Research Center
  National Aeronautics and Space Administration
   *Edwards, California 93523*
      September 10, 1975

APPENDIX A

TRANSFORMATION OF ANGLE OF SIDESLIP
FROM NOSE BOOM AXIS TO WIND AXIS

An equation can be derived to transform the vane-measured angle of sideslip from the nose boom axis to the wind axis.

In figure 24, let x, y, and z represent the coordinates of the nose boom body axes with origin at 0. Let V be the wind-axis-oriented velocity vector, with components u, v, and w relative to the body axis. Finally, let β_i be the angle of sideslip measured by the angle of sideslip vane with respect to the nose boom axis, $\beta_i{}^*$ the vane angle of sideslip with respect to the wind axis, and α_t the angle of attack of the nose boom.
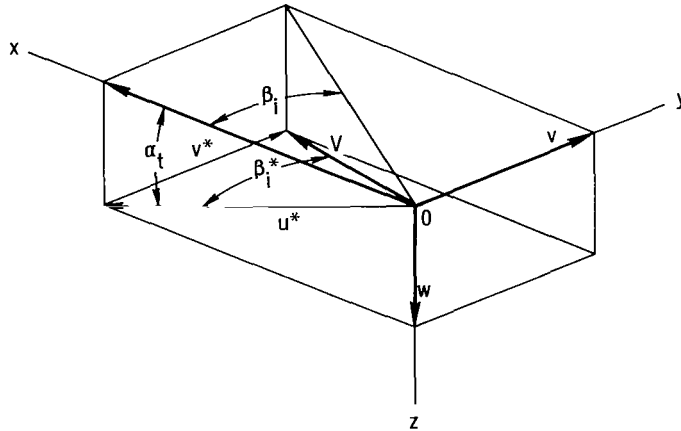
*Figure 24. Velocity vector diagram used for derivation
of angle of sideslip axis transformation.*

With respect to $\beta_i{}^*$, the velocity components are as follows:

$$u^* = V \cos \beta_i{}^* \tag{1}$$

$$v^* = V \sin \beta_i{}^* \tag{2}$$

The velocity components u^* and v^* are resolved in the x–y plane as follows:

$$u = u^* \cos \alpha_t$$

or

$$u = V \cos \beta_i^* \cos \alpha_t \qquad (3)$$

and

$$v = v^*$$

or

$$v = V \sin \beta_i^* \qquad (4)$$

The indicated angle of sideslip as measured by the angle of sideslip vane with respect to the nose boom axis is defined as follows:

$$\tan \beta_i = \frac{v}{u} \qquad (5)$$

From equations (3) to (5),

$$\tan \beta_i = \frac{V \sin \beta_i^*}{V \cos \beta_i^*} \cos \alpha_t = \frac{\tan \beta_i^*}{\cos \alpha_t}$$

or

$$\tan \beta_i^* = \tan \beta_i \cos \alpha_t \qquad (6)$$

Applying the small angle approximation to equation (6), that is, $\tan \beta_i^* \approx \beta_i^*$ and $\tan \beta_i \approx \beta_i$, equation (6) becomes

$$\beta_i^* = \beta_i \cos \alpha_t$$

32

APPENDIX B

CALIBRATION DATA SUMMARY

Angle of Attack

Figure 25 summarizes the angle of attack vane calibration in three-dimensional plots for the Mach numbers tested. The vane aerodynamic characteristics are presented in terms of the vane position error (vertical graduations) at constant angles of attack for various angles of sideslip. The data are connected by solid or broken lines to indicate positive and negative errors, respectively, and to form the error network. Vertical bars from above and below the baseline to the data represent the magnitude of the vane error. For Mach numbers at which the vane errors are quasilinear or the vanes are free of shock interference, the error network appears as a plane surface. For Mach numbers at which shock waves interfere with the vanes, the interactions appear as warped surfaces (figs. 25(l) to 25(n)). Interactions occur at Mach numbers above 2.00.

(a) $M_\infty = 0.40$.

(b) $M_\infty = 0.60$.
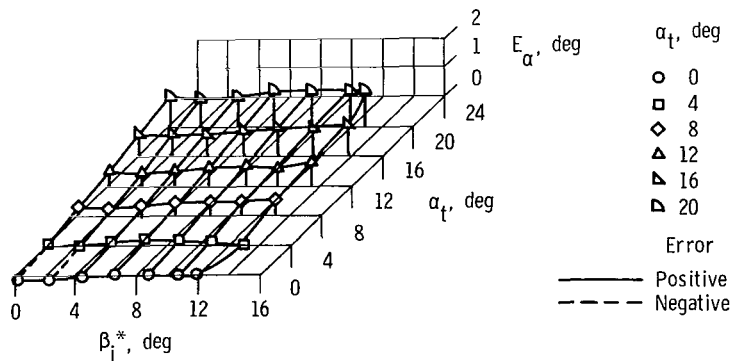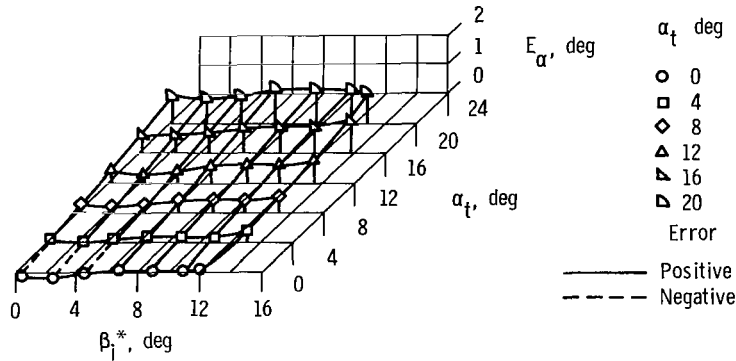
Figure 25. Three-dimensional parametric description of angle of attack vane error variation at constant Mach number.
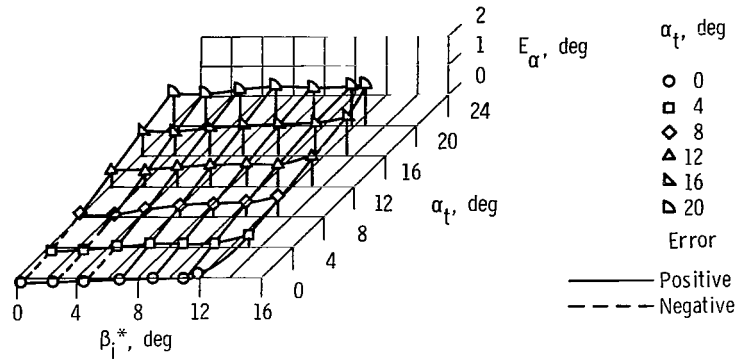
(c) $M_\infty = 0.80$.
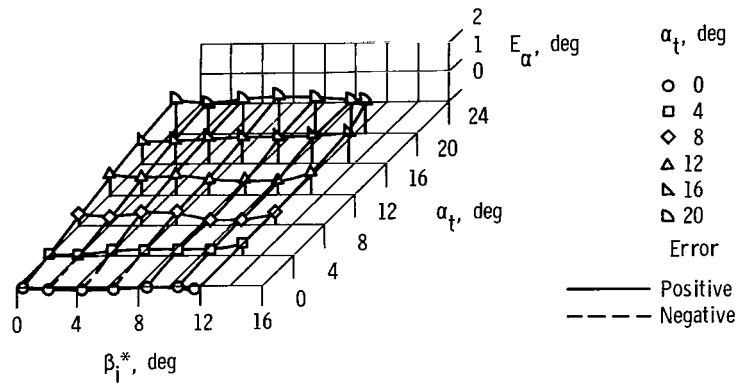
(d) $M_\infty = 0.90$.
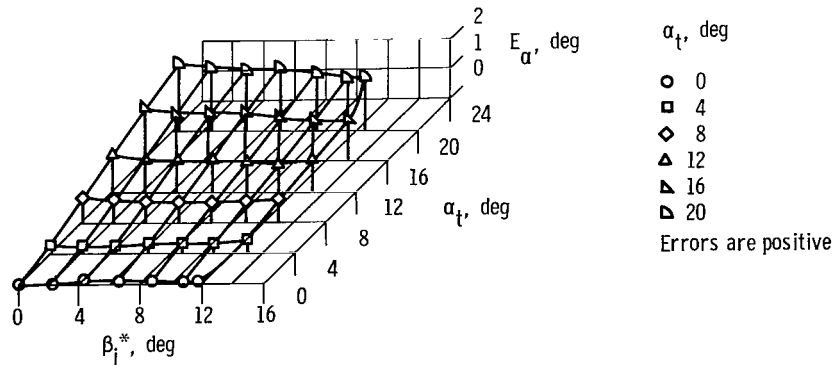
(e) $M_\infty = 0.95$.

Figure 25. Continued.
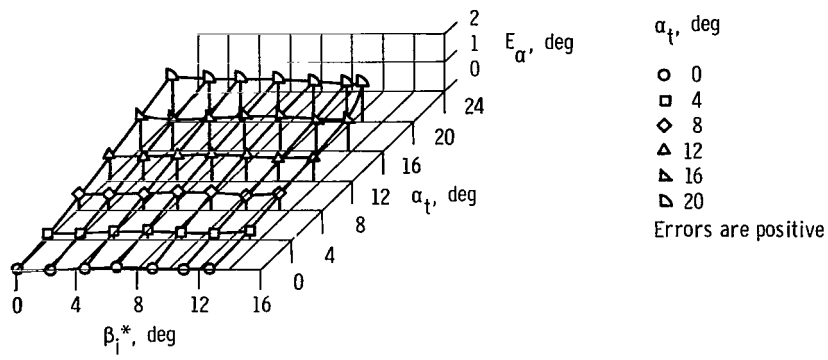
(f) $M_\infty = 1.05$.
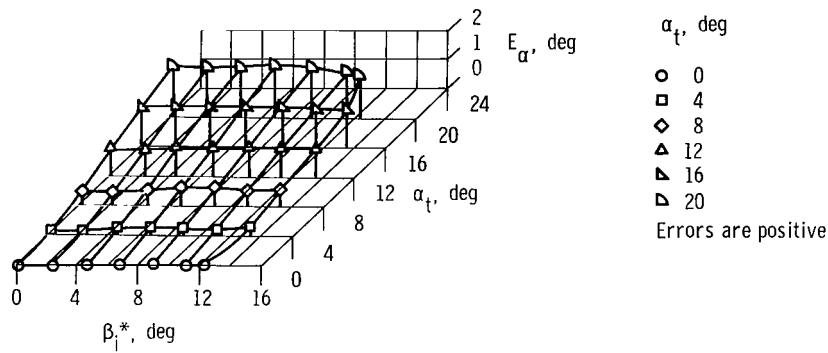
(g) $M_\infty = 1.10$.
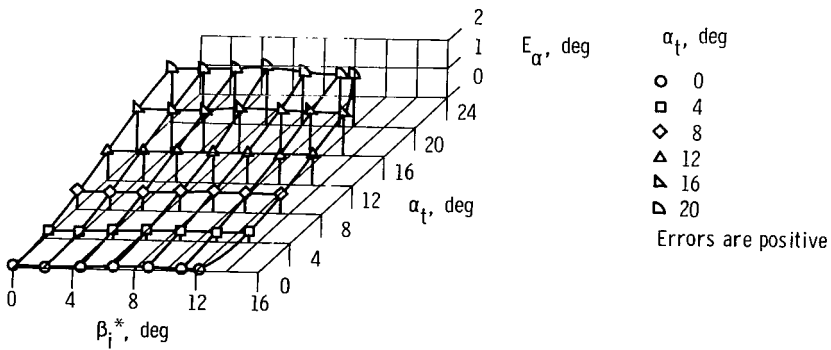
(h) $M_\infty = 1.20$.

Figure 25. Continued.
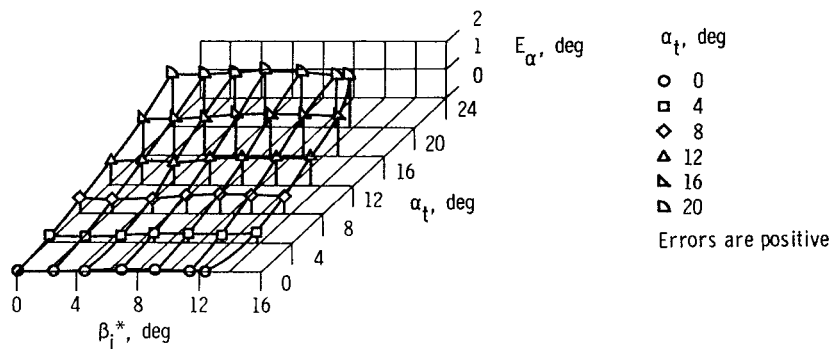
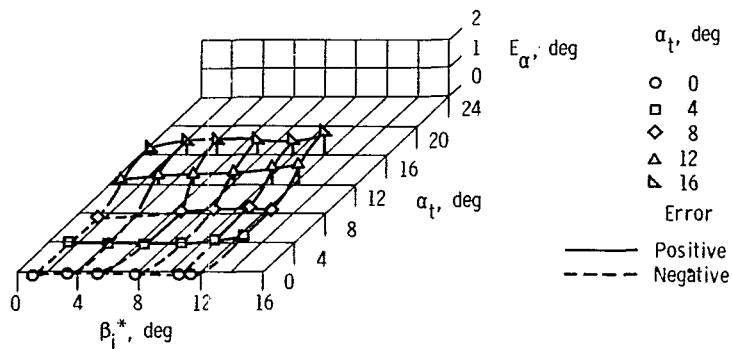(i) $M_\infty = 1.30$.
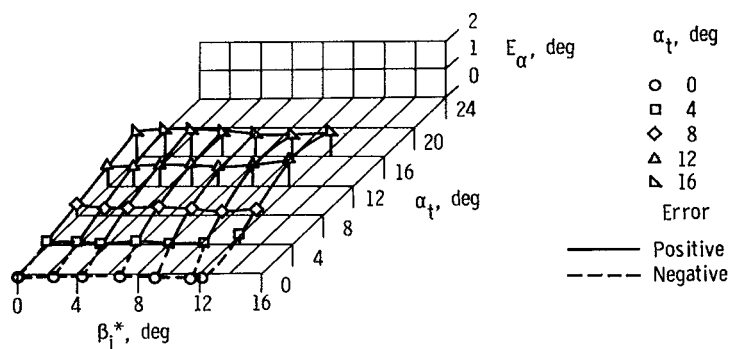
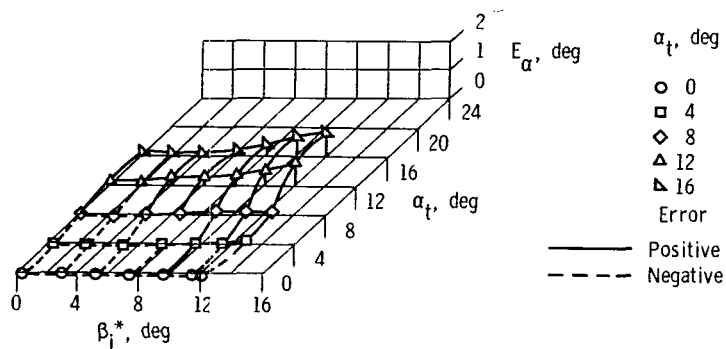(j) $M_\infty = 1.51$.
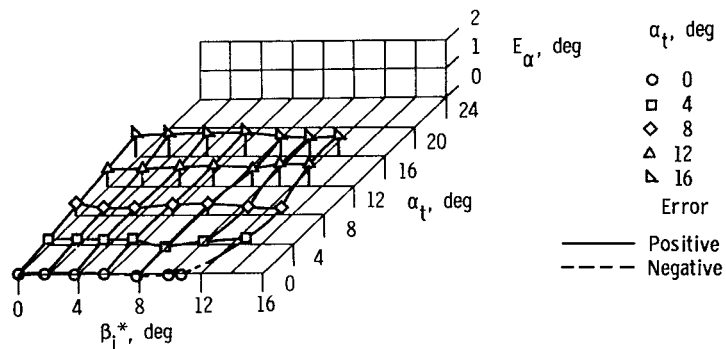
(k) $M_\infty = 1.91$.

Figure 25. Continued.
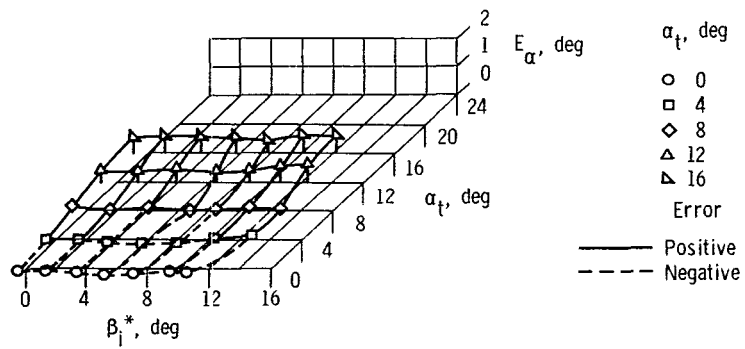
(l) $M_\infty = 2.11$.

(m) $M_\infty = 2.31$.

(n) $M_\infty = 2.54$.

Figure 25.   Concluded.

Angle of Sideslip

Figure 26 summarizes the angle of sideslip vane calibration in three-dimensional plots for the Mach numbers tested. The three-dimensional parametric descriptions of the vane aerodynamic characteristics are constructed like the angle of attack vane error descriptions in figure 25. For the Mach numbers at which the vane is free of shock interference, the vane error network remains a plane surface. Once shock interference occurs, beginning with $M_\infty = 1.20$ at angles of attack above 10°, the character of the surface changes for each succeeding Mach number. The degree of distortion is indicative of the severity of the interference of the shocks with the vane.

The surfaces in figure 26 as well as those in figure 25 effectively depict the aerodynamic characteristics of the angle of sideslip and angle of attack vanes in terms of the Mach numbers at which shock-to-vane interactions occur, but they do not identify the origins of the shock systems. The analysis presented in figure 16 is more useful for identifying the shock systems that interact with the vanes.

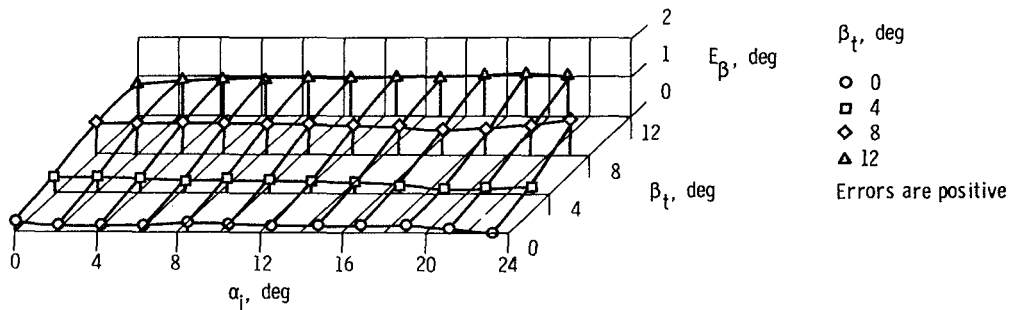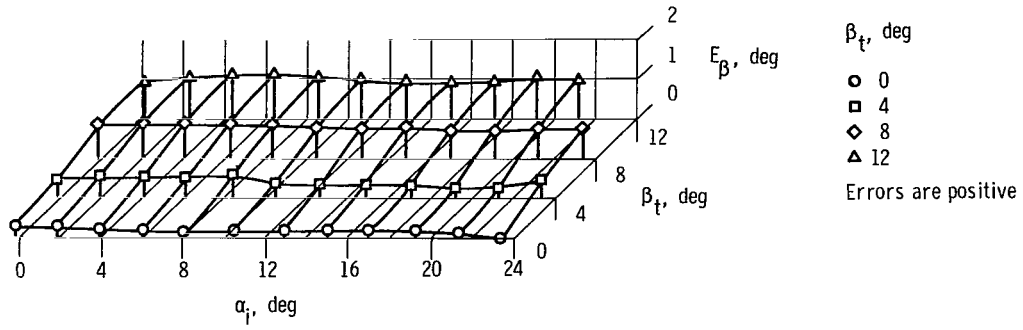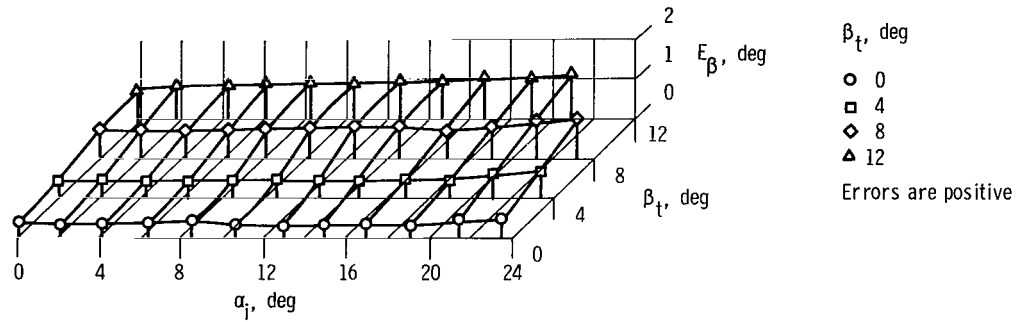*(a)* $M_\infty = 0.40$.

(b) $M_\infty = 0.60$.
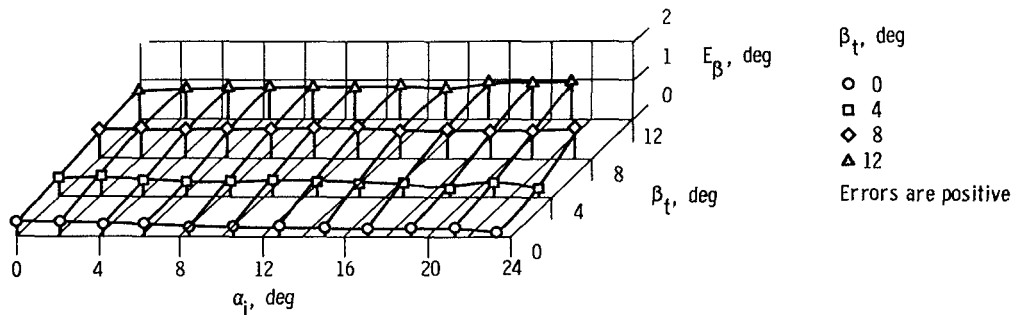
Figure 26.   Three-dimensional parametric description of angle of sideslip vane error variation at constant Mach number.
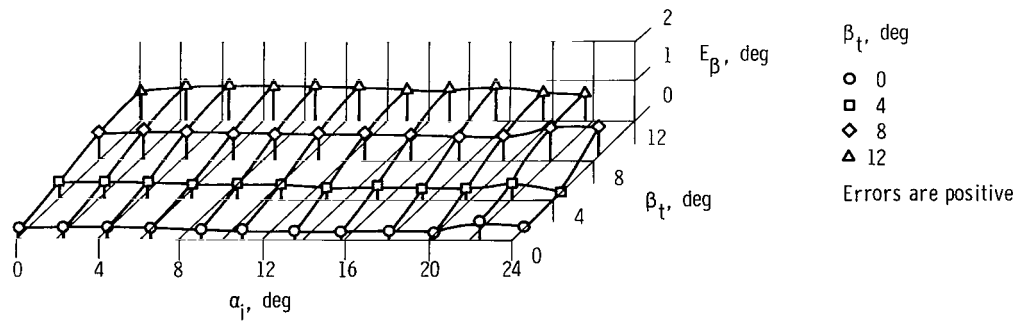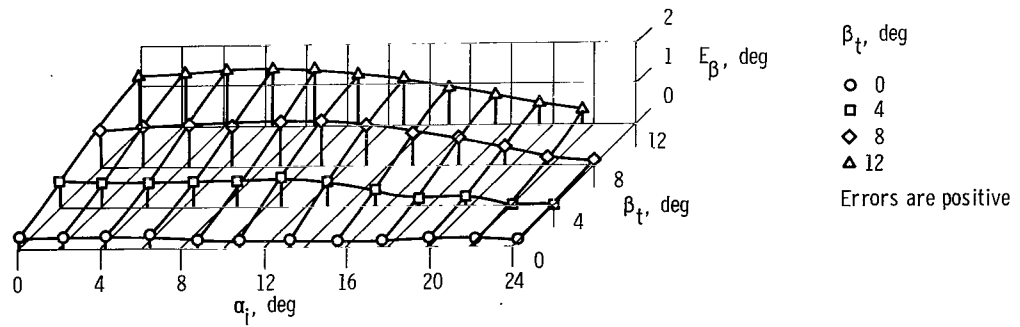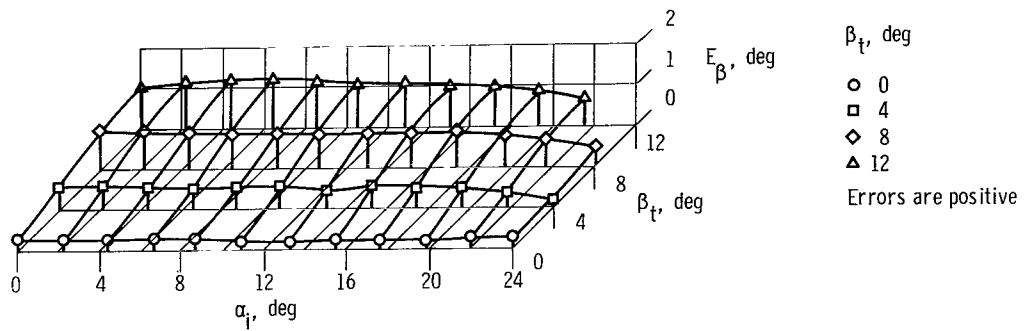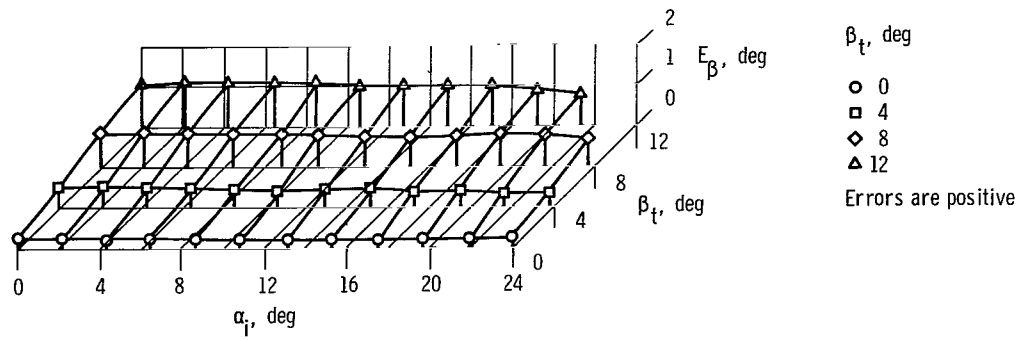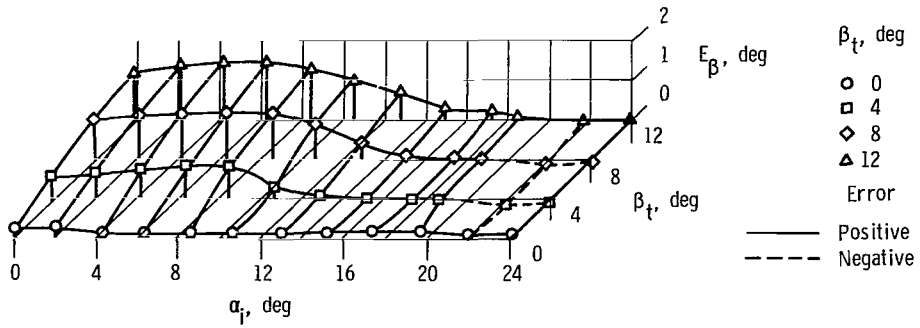
(c) $M_\infty = 0.80$.

(d) $M_\infty = 0.90$.

(e) $M_\infty = 0.95$.

Figure 26. Continued.

(f) $M_\infty = 1.05$.

(g) $M_\infty = 1.10$.

(h) $M_\infty = 1.20$.
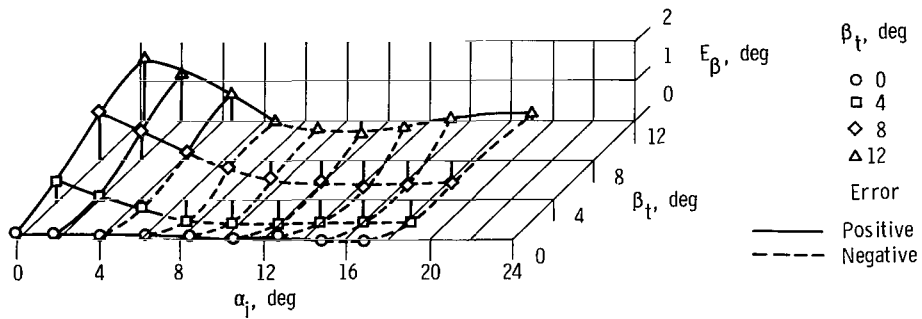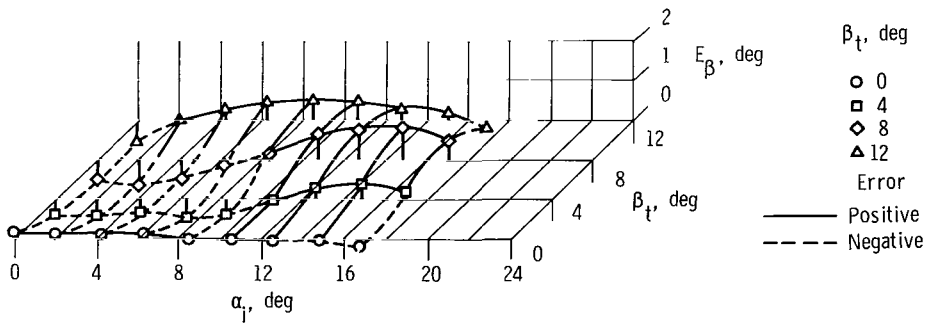
Figure 26. Continued.
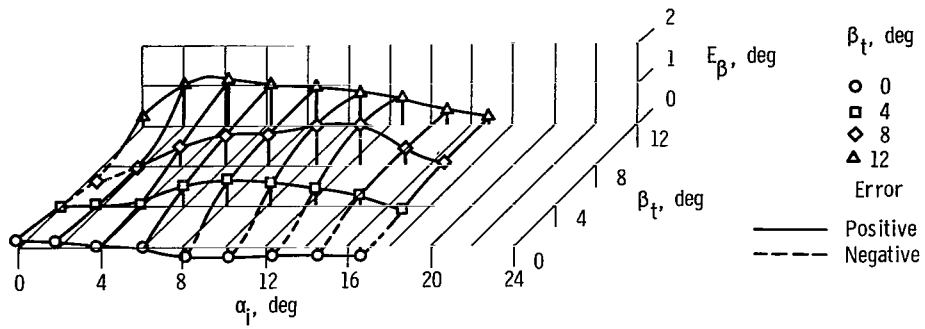
(i) $M_\infty = 1.30$.

(j) $M_\infty = 1.51$.
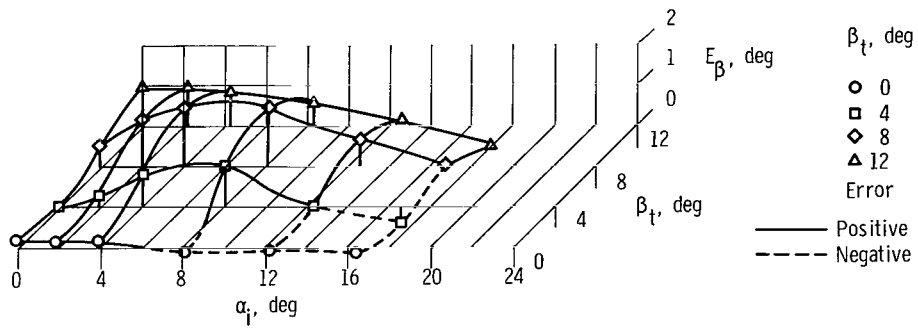

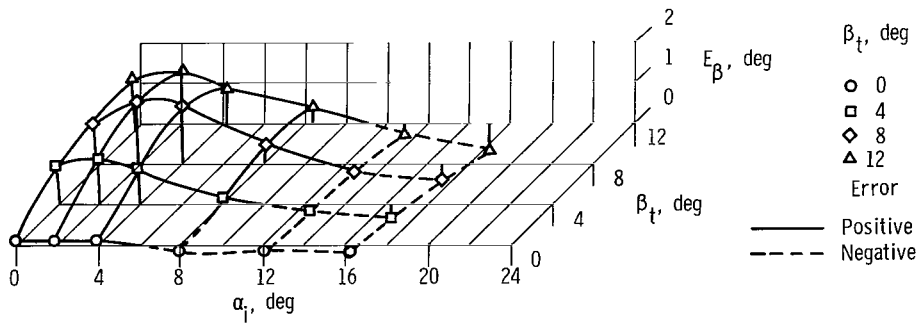(k) $M_\infty = 1.91$.

Figure 26. Continued.

41

(l) $M_\infty = 2.11$.

(m) $M_\infty = 2.31$.

(n) $M_\infty = 2.54$.

Figure 26. Concluded.

42

REFERENCES

1. Pearson, Albin O.; and Brown, Harold A.: Calibration of a Combined Pitot-Static Tube and Vane-Type Flow Angularity Indicator at Transonic Speeds and at Large Angles of Attack or Yaw. NACA RM L52F24, 1952.

2. Sinclair, Archibald R.; and Mace, William D: Wind-Tunnel Calibration of a Combined Pitot-Static Tube and Vane-Type Flow-Angularity Indicator at Mach Numbers of 1.61 and 2.01. NACA TN 3808, 1956.

3. Richardson, Norman R.; and Pearson, Albin O: Wind-Tunnel Calibrations of a Combined Pitot-Static Tube, Vane-Type Flow-Direction Transmitter, and Stagnation-Temperature Element at Mach Numbers From 0.60 to 2.87. NASA TN D-122, 1959.

4. Uselton, James C.; and Shadow, T. O.: Results of Wind Tunnel Tests on a Flight Path Accelerometer at Mach Numbers From 0.2 to 3.0. AEDC-TR-71-260, Arnold Engineering Dev. Center, Feb. 1972.

5. Shadow, T. O.: Wind Tunnel Investigation of the Transonic Aerodynamic Characteristics of a Full-Scale Flight Path Accelerometer (Follow-On Tests). AEDC-TR-72-1, Arnold Engineering Dev. Center, Feb. 1972.

6. Uselton, James C.: Wind Tunnel Test Results on a Flight Path Accelerometer at Subsonic and Supersonic Speeds. AEDC-TR-72-45, Arnold Engineering Dev. Center, June 1972.

7. Mechtly, E. A.: The International System of Units — Physical Constants and Conversion Factors. Second Revision. NASA SP-7012, 1973.

8. Perrelle, C. J.; Hardin, R. D.; Heckart, M. V.; and Brown, K. R.: An Inventory of Aeronautical Ground Research Facilities. Volume 3: Structural. NASA CR-1874, 1971.

9. Allen, H. Julian; and Perkins, Edward W.: A Study of Effects of Viscosity on Flow Over Slender Inclined Bodies of Revolution. NACA TR 1048, 1951.

10. Yaggy, Paul F.: A Method for Predicting the Upwash Angles Induced at the Propeller Plane of a Combination of Bodies With an Unswept Wing. NACA TN 2528, 1951.

11. Rogallo, Vernon L.: Effects of Wing Sweep on the Upwash at the Propeller Planes of Multiengine Airplanes. NACA TN 2795, 1952.

12. Woodward, F. A.: Analysis and Design of Wing-Body Combinations at Subsonic and Supersonic Speeds. J. Aircraft, vol. 5, no. 6, Nov.-Dec. 1968, pp. 528-534.

"The aeronautical and space activities of the United States shall be conducted so as to contribute . . . to the expansion of human knowledge of phenomena in the atmosphere and space. The Administration shall provide for the widest practicable and appropriate dissemination of information concerning its activities and the results thereof."
— NATIONAL AERONAUTICS AND SPACE ACT OF 1958

NASA SCIENTIFIC AND TECHNICAL PUBLICATIONS

TECHNICAL REPORTS: Scientific and technical information considered important, complete, and a lasting contribution to existing knowledge.

TECHNICAL NOTES: Information less broad in scope but nevertheless of importance as a contribution to existing knowledge.

TECHNICAL MEMORANDUMS: Information receiving limited distribution because of preliminary data, security classification, or other reasons. Also includes conference proceedings with either limited or unlimited distribution.

CONTRACTOR REPORTS: Scientific and technical information generated under a NASA contract or grant and considered an important contribution to existing knowledge.

TECHNICAL TRANSLATIONS: Information published in a foreign language considered to merit NASA distribution in English.

SPECIAL PUBLICATIONS: Information derived from or of value to NASA activities. Publications include final reports of major projects, monographs, data compilations, handbooks, sourcebooks, and special bibliographies.

TECHNOLOGY UTILIZATION PUBLICATIONS: Information on technology used by NASA that may be of particular interest in commercial and other non-aerospace applications. Publications include Tech Briefs, Technology Utilization Reports and Technology Surveys.

Details on the availability of these publications may be obtained from:

SCIENTIFIC AND TECHNICAL INFORMATION OFFICE

NATIONAL AERONAUTICS AND SPACE ADMINISTRATION

Washington, D.C. 20546